ELSEVIER

ADVANCES IN COLLOID AND INTERFACE SCIENCE

Advances in Colloid and Interface Science
85 (2000) 145–192

www.elsevier.nl/locate/cis

Capillary interactions between particles bound to interfaces, liquid films and biomembranes

Peter A. Kralchevsky [a,b], Kuniaki Nagayama[a,*]

[a] *Laboratory of Ultrastructure Research, National Institute for Physiological Sciences, Myodaiji-cho, Okazaki 444-8585, Japan*
[b] *Laboratory of Thermodynamics and Physicochemical Hydrodynamics, Faculty of Chemistry, University of Sofia, Sofia 1126, Bulgaria*

Abstract

This article is devoted to an overview, comparison and discussion of recent results (both theoretical and experimental) about lateral capillary forces. They appear when the contact of particles or other bodies with a fluid phase boundary causes perturbations in the interfacial shape. The capillary interaction is due to the overlap of such perturbations which can appear around floating particles, vertical cylinders, particles confined in a liquid film, inclusions in the membranes of lipid vesicles or living cells, etc. In the case of floating particles the perturbations are due to the particle weight; in this case the force decreases with the sixth power of the particle size and becomes immaterial for particles smaller than approximately 10 μm. In all other cases the interfacial deformations are due to the particle wetting properties; the resulting 'immersion' capillary forces can be operative even between very small particles, like protein globules. In many cases such forces can be responsible for the experimentally observed two-dimensional particle aggregation and ordering. An analogy between capillary and electrostatic forces enables one to introduce 'capillary charges' of the attached particles, which characterize the magnitude of the interfacial deformation and could be both positive and negative. Moreover, the capillary interaction between particle and wall resembles the image force in electrostatics. When a particle is moving bound to an interface under the action of a capillary force, one can determine the surface drag

* Corresponding author. Tel: +81-564-55-7811; fax: + 81-564-52-7913.
E-mail address: nagayama@nips.ac.jp (K. Nagayama).

PII: S0001-8686(99)00016-0

coefficient and the surface viscosity supposedly the magnitude of the capillary force is known. Alternative (but equivalent) energy and force approaches can be used for the theoretical description of the lateral capillary interactions. Both approaches require the Laplace equation of capillarity to be solved and the meniscus profile around the particles to be determined. The energy approach accounts for contributions due to the increase of the meniscus area, gravitational energy and/or energy of wetting. The second approach is based on calculating the net force exerted on the particle, which can originate from the hydrostatic pressure, interfacial tension and bending moment. In the case of small perturbations, the superposition approximation can be used to derive an asymptotic formula for the capillary forces, which has been found to agree well with the experiment. Capillary interactions between particles bound to spherical interfaces are also considered taking into account the special geometry and restricted area of such phase boundaries. A similar approach can be applied to quantify the forces between inclusions (transmembrane proteins) in lipid membranes. The deformations in a lipid membrane, due to the inclusions, can be described theoretically in the framework of a mechanical model of the lipid bilayer, which accounts for its 'hybrid' rheology (neither elastic body nor fluid). In all considered cases the lateral capillary interaction originates from the overlap of interfacial deformations and is subject to a unified theoretical treatment, despite the fact that the characteristic particle size can vary from 1 cm down to 1 nm.

Keywords: Capillary forces; Lipid membranes containing inclusions; Liquid films containing particles; Surface viscosity measurements; Two-dimensional aggregation

Contents

1. Introduction

It is known from the experiment and practice that particles floating on a fluid interface attract each other and form clusters. Such effects are observed and utilized in some extraction and separation flotation processes [1,2]. As noticed by Nicolson [3] these lateral capillary forces are caused by the deformation of the interface due to the effect of gravity (particle weight and buoyancy force). The shape of the surface deformations created by floating particles has been studied by Hinsch [4] by means of a holographic method. Allain and Jouhier [5], and in other experiment Allain and Cloitre [6], have studied the aggregation of spherical particles floating at the surface of water and demonstrated that the obtained aggregates have a structure corresponding to a fractal dimension 1.6. A theoretical calculation of the capillary force between two vertical or inclined plates, partially immersed in a liquid, has been carried out by Derjaguin and Starov [7].

Our interest in the capillary forces was provoked by the finding that small colloidal particles and protein macromolecules confined in liquid films also exhibit attraction and do form clusters and larger ordered domains (two-dimensional arrays) [8–13]. However, the weight of such tiny particles is too small to create any surface deformation. Nevertheless, they also produce interfacial deformations because of their confinement in the liquid film; such deformations depend on the wetting properties of particle surfaces related to the thermodynamic requirement that the interface must meet the particle surface at a given angle — the contact angle. The overlap of such wetting-driven deformations also gives rise to a lateral capillary force [14].

After Nicolson [3], who derived an approximated analytical expression for the capillary force between two floating bubbles, calculations about the capillary force per unit length of two infinite parallel horizontal floating cylinders were carried out by Gifford and Scriven [15] and by Fortes [16]. This configuration is the simplest one, because the meniscus has a translational symmetry and the Laplace equation, governing the interfacial profile, acquires a simpler form [7,15,16]. Chan et al. [17] derived analytical expressions for floating horizontal cylinders and spheres using the Nicolson's superposition approximation, whose validity was supported by a comparison with the exact numerical results for cylinders from Gifford and Scriven [15].

The aforementioned studies [3,15–17] deal with floating particles. For the first time the capillary forces between two vertical cylinders and between two spheres

partially immersed (confined) in a liquid layer have been theoretically studied by Kralchevsky et al. [14]. A general expression for the interaction energy has been used [14], which includes contributions from the gravitational energy, energy of particle wetting and energy of increase of the meniscus area due to the deformation caused by the particles; this expression is valid for both floating and confined particles. Expressions and numerical results for the energy and force of interaction have been obtained for the case when the slope of the deformed meniscus is small; this case corresponds to the usual experimental situation with small particles. The theory has been extended also to particles entrapped in thin films, for which the disjoining pressure effect, rather than gravity, keeps the non-deformed surface planar [14].

Another new moment in the paper by Kralchevsky et al. [14] is the approach to solving the Laplace equation: instead of assuming a mere superposition of the known axisymmetric profiles around two separate particles, the linearized Laplace equation has been solved directly in bipolar coordinates, which allows one to impose the correct boundary conditions at the particle contact lines (constancy of the contact angle). Thus a correct theoretical description of the force at small interparticle distances is achieved, which is not accessible to the superposition approximation.

Paunov et al. [18] obtained solutions for the meniscus profile in bipolar coordinates for other configurations: vertical cylinder–vertical wall, and particle–vertical wall. A different, *force* approach to the calculation of lateral capillary interactions has been applied to obtain both analytical and numerical results. The validity of the derived analytical expressions has been confirmed by checking whether the force exerted on the particle and the wall have equal magnitudes and opposite signs, as required by the third Newton's law.

Next, the theory developed by Kralchevsky et al. [14] and Paunov et al. [18] was extended in [19] in the following two aspects. First, the *energy* approach and the *force* approach have been applied to the same object: vertical cylinders and particles in a liquid film; the two approaches were found to give numerically coinciding results, although their equivalence has not been proven analytically there. Furthermore, in Ref. [19] an analytical solution of Laplace equation in bipolar coordinates has been obtained for the case of two *dissimilar* particles: vertical cylinders and/or spheres confined in a film. Attractive and repulsive capillary forces have been obtained depending on whether the meniscus slope at the contact line of the two particles has similar or different signs.

In Ref. [20] the theory of the capillary forces between small *floating* particles of different size has been extended on the basis of the result for the meniscus profile from Ref. [19]. The energy approach has been applied to calculate the capillary interaction, appropriate analytical expressions have been derived and numerical results for various configurations have been obtained. From the general expression for the interaction free energy the approximation of Nicolson [3] has been derived as an asymptotic case, and thus its validity has been proven analytically. It has been noticed that in a wide range of distances the capillary forces obey a two-dimensional version of the Coulomb law of electricity. Following this analogy 'capillary

charges' of the particles have been introduced; depending on whether the two 'capillary charges' have the same or the opposite sign, the capillary force is respectively attractive or repulsive.

In Ref. [20] the physical nature and the magnitude of the lateral capillary forces between floating and confined particles have been compared and the differences between them have been explicitly analyzed. It has been established that the energy of capillary interaction between floating particles becomes negligible (smaller than the thermal energy kT) for particles smaller than 5–10 μm. On the other hand, when the particles (instead of being freely floating) are partially immersed into a liquid film, the energy of capillary interaction is much larger (for the same particle size), and it can be much greater than kT even for particles of nanometer size. This analysis has been extended in Ref. [21], where the former type of capillary interactions have been called 'flotation forces', and the latter — 'immersion forces'. Other configurations have been also investigated in Ref. [21]: (i) two particles in a symmetric liquid film with account for the disjoining pressure effect, and (ii) two particles of fixed contact lines (rather than fixed contact angles). It has been established that the interaction at fixed contact angle is stronger than that at fixed contact line. Finally, in Ref. [21] the equivalence of the energy and force approaches to the capillary interactions has been analytically proven for the case of two semi-immersed vertical cylinders.

Paunov et al. [18] noticed that the meniscus between a vertical cylinder (or particle) and a wall has the same shape as the meniscus between two identical particles, each of them being the image of the other one with respect to the wall. For that reason the capillary interaction between the particle and the wall is the same as between the particle and its mirror image. In this respect there is analogy with the image forces in electrostatics. This idea has been applied and developed in Refs. [22,23], where the capillary image forces between particles floating over an inclined meniscus in a vicinity of a wall have been theoretically and experimentally investigated.

Further extension of the theory of capillary forces has been achieved in Ref. [24], where the interaction between particles attached to a spherical interface (membrane) has been carried out; note that in contrast with the planar interface (or film) the spherical interface has a finite area and 'infinite' interparticle separations are not possible. Other extension of the theory has been made by Kralchevsky et al. [25], where lateral capillary forces between inclusions in phospholipid membranes have been investigated on the basis of a special mechanical model accounting for the elastic properties of the lipid bilayer. It is a general conclusion from all studies of lateral immersion forces is that they are strong enough to produce aggregation and ordering of sub-micrometer particles [14,18–25]. This fact could explain numerous experimental evidences about the formation of two-dimensional (2D) particle arrays in liquid films [26–45] and in phospholipid membranes [46–48].

It should be also noted, that the problem about horizontal floating cylinders, was reexamined by Allain and Cloitre [49,50], who used the linear superposition approximation and alternatively, a more rigorous expressions for the free energy of

the cylinders; they calculated the capillary force for both light and heavy cylinders (for both small and large Bond numbers).

We should note that the lateral capillary forces are distinct from the popular *capillary bridge forces*, which are known to form contacts between particles in the soil, pastes, as well as in some experiments with the atomic force microscope (AFM), see e.g. Mate et al. [51–56]. The capillary bridge forces act normally to the plane of the contact line on the particle surface, whereas the lateral capillary forces are directed (almost) tangentially to the plane of the contact line.

Lucassen [57] proposed another type of capillary force, which can be operative between *particles of irregular wetting perimeter*. The latter creates respective irregular deformations in the surrounding liquid surface, even if the weight of the particle is negligible. The overlap of the deformations around such two particles also gives rise to a lateral capillary force. For the time being only a single theoretical study [57] of this kind of forces has been carried out.

In Section 2 we give an outline of the main results (both theoretical and experimental) for flotation and immersion lateral capillary forces. Then we demonstrate how the asymptotic expressions for these forces are derived. Further, we review the extension of the theory to particles at spherical interfaces/films and to inclusions in lipid bilayers.

2. Overview of results about lateral capillary forces

2.1. Interaction between two particles

As mentioned in the introduction, the origin of the lateral capillary forces is the *deformation* of the liquid surface, which is supposed to be flat in the absence of particles. The larger the interfacial deformation created by the particles, the stronger the capillary interaction between them. It is known that two similar particles floating on a liquid interface attract each other [3,15–17,20,21] — see Fig. 1a. This attraction appears because the liquid meniscus deforms in such a way that the gravitational potential energy of the two particles decreases when they approach each other. Hence the origin of this force is the *particle weight* (including the Archimedes force).

A force of capillary attraction appears also when the particles (instead of being freely floating) are partially immersed (confined) into a liquid layer [14,18,19,21,24] — see Fig. 1b. The deformation of the liquid surface in this case is related to the *wetting properties* of the particle surface, i.e. to the position of the contact line and the magnitude of the contact angle, rather than to gravity.

To make a difference between the capillary forces in the case of floating particles and in the case of particles immersed in a liquid film, the former are called lateral *flotation* forces and the latter — lateral *immersion* forces [20,21]. These two kinds of force exhibit similar dependence on the interparticle separation but very different dependencies on the particle radius and the surface tension of the liquid. The flotation and immersion forces can be both attractive (Fig. 1a,b)

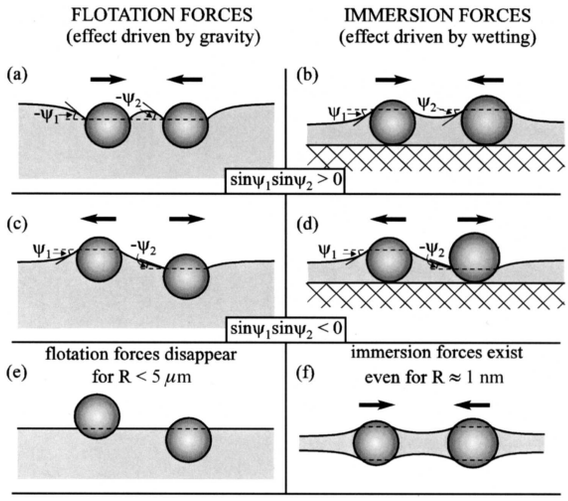

Fig. 1. Capillary forces of flotation (a,c,e) and immersion (b,d,f) type: (a) attraction between two similar floating particles; (b) attraction between two similar particles immersed in a liquid film on a substrate; (c) repulsion between a light and a heavy floating particle; (d) repulsion between a hydrophilic and a hydrophobic particle; (e) small floating particles do not deform the interface and do not interact, (f) small particles confined within a liquid film experience capillary interaction because they deform the film surfaces due to the effects of wetting [21].

and repulsive (Fig. 1c,d). This is determined by the signs of the meniscus slope angles ψ_1 and ψ_2 at the two contact lines: the capillary force is attractive when $\sin\psi_1 \sin\psi_2 > 0$ and repulsive when $\sin\psi_1 \sin\psi_2 < 0$. In the case of flotation forces $\psi > 0$ for *light* particles (including bubbles) and $\psi < 0$ for *heavy* particles. In the case of immersion forces between particles protruding from an aqueous layer $\psi > 0$ for *hydrophilic particles* and $\psi < 0$ for *hydrophobic particles*. When $\psi = 0$ there is no meniscus deformation and, hence, there is no capillary interaction between the particles. This can happen when the weight of the particles is too small to create a significant surface deformation, Fig. 1e. The immersion force appears not only between particles in wetting films (Fig. 1b,d), but also in symmetric fluid films (Fig. 1f). The theory [17,20–22] provides the following asymptotic expression for calculating the lateral capillary force between two particles of radii R_1 and R_2 separated by a center-to-center distance L.

$$F = -2\pi\sigma Q_1 Q_2 q \mathrm{K}_1(qL)\left[1 + O(q^2 R_k^2)\right] \qquad r_k \ll L \tag{2.1}$$

where σ is the liquid–fluid interfacial tension, r_1 and r_2 are the radii of the two contact lines and

$$\mathrm{Q}_i = r_i \sin\psi_i \qquad (i = 1,2) \tag{2.2}$$

is the 'capillary charge' of the particle [20–22]; in addition

$$q^2 = \Delta\rho g/\sigma \quad \text{(in thick film)}$$
$$q^2 = (\Delta\rho g - \Pi')/\sigma \quad \text{(in thin films)} \tag{2.3}$$

Here $\Delta\rho$ is the difference between the mass densities of the two fluids and Π' is the derivative of the disjoining pressure with respect to the film thickness; $K_1(x)$ is the modified Bessel function (or Macdonald function) of the first order [58–60]. The derivation of Eqs. (2.1) and (2.3) can be found in Section 3. The asymptotic form of Eq. (2.1) for $qL \ll 1$ ($q^{-1} = 2.7$ mm for water),

$$F = -2\pi\sigma Q_1 Q_2/L \quad r_k \ll L \ll q^{-1} \tag{2.4}$$

looks like a two-dimensional analogue of Coulomb's law, which explains the name 'capillary charge' of Q_1 or Q_2. It is worth noting that the immersion and flotation forces exhibit the same functional dependence on the interparticle distance, see Eqs. (2.1) and (2.4). On the other hand, their different physical origin results in different magnitudes of the 'capillary charges' of these two kinds of capillary force. In this respect they resemble the electrostatic and gravitational forces, which obey the same power law, but differ in the physical meaning and magnitude of the force constants (charges, masses). In the particular case when $R_1 = R_2 = R$; $r_k \ll L \ll q^{-1}$ one can derive [20,21,61]

$$F \propto (R^6/\sigma)K_1(qL) \quad \text{for flotation force}$$
$$F \propto \sigma R^2 K_1(qL) \quad \text{for immersion force} \tag{2.5}$$

Consequently, the flotation force decreases, while the immersion force increases, when the interfacial tension σ increases. Besides, the flotation force decreases much stronger with the decrease of R than the immersion force. Thus $F_{\text{flotation}}$ is negligible for $R < 5$–10 μm, whereas $F_{\text{immersion}}$ can be significant even when $R = 2$ nm, see Fig. 2. (Protein molecules of nanometer size can be considered as 'particles' insofar as they are much larger than the solvent (water) molecules.) In Fig. 2 the two types of capillary interaction are compared, with respect to their energy $\Delta W(L) = \int_L^\infty F(L')\mathrm{d}L'$, for a wide range of particle sizes. The values of the parameters used are: particle mass density $\rho_p = 2$ g/cm^3, density difference between the two fluids $\Delta\rho = 1$ g/cm^3, surface tension $\sigma = 40$ mN/m, contact angle $\alpha = 60°$, interparticle distance $L = 2R$, and thickness of the non-disturbed planar film $l_0 = R$. The pronounced difference in the magnitudes of the two types of capillary forces is due to the different magnitude of the interfacial deformation. The small floating particles are too light to create a substantial deformation of the liquid surface and the lateral capillary force is negligible. In the case of immersion forces the particles are restricted in the vertical direction by the solid substrate (Fig. 1b) or by the two surfaces of the liquid film (Fig. 1f). Therefore, as the film becomes thinner, the liquid surface deformation increases, thus giving rise to a

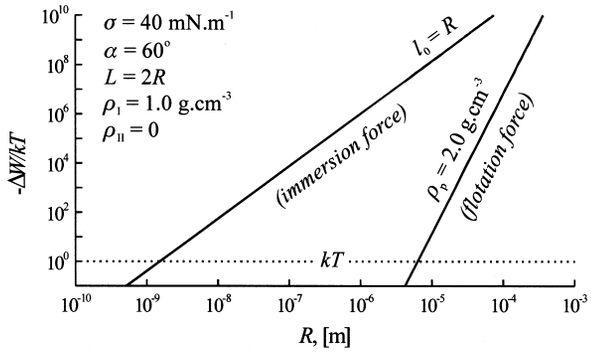

Fig. 2. Energy of capillary attraction ΔW, in kT units, plotted vs. the radius R of two similar particles separated at a center-to-center distance $L = 2R$. If $|\Delta W| > kT$, the capillary attraction is stronger than the Brownian force and can cause particle aggregation [20,21]

strong interparticle attraction. Hence, as already mentioned, the immersion forces may be one of the main factors causing the observed self assembly of small colloidal particles [11–13,26–45] and protein macromolecules confined in thin liquid films [8–10] or lipid bilayers [25,46–48].

In the case of interactions between inclusions in lipid bilayers (Fig. 3) the elasticity of the bilayer interior must also be taken into account. The calculated energy of capillary interaction between integral membrane proteins turns out to be of the order of several kT; hence, such an interaction can be one possible explanation of the observed aggregation of membrane proteins [25,48]. Lateral capillary forces can be operative also between particles captured in a *spherical* (rather than planar) thin liquid film or lipid vesicle [24].

2.2. Measurements of lateral capillary forces

The first measurement of lateral capillary force (of the immersion type) has been carried out by Camoin et al. [62] with millimeter-sized polystyrene spheres attached to the tip of rod-like holders. By means of a sensitive electromechanical balance it has been established that the force is attractive and decays (approx.) exponentially,

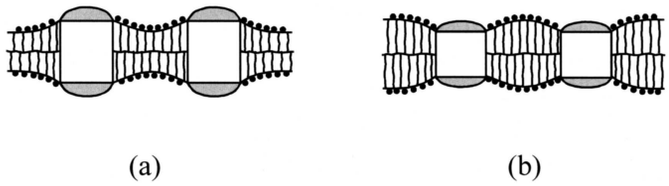

Fig. 3. The thickness of an inclusion (say transmembrane protein) can be (a) greater or (b) smaller than the thickness of the non-disturbed phospholipid bilayer. In both cases the overlap of the deformations around two similar inclusions gives rise to attraction between them.

which corresponds to the long-distance asymptotics of Eq. (2.1), see e.g. Lucassen [59]and Dwight [63]:

$$F \approx -\pi Q_1 Q_2 \left(\frac{2\pi q}{L}\right)^{1/2} \exp(-qL)\left[1 + O\left(\frac{1}{qL}\right)\right] \quad (qL \geq 2) \tag{2.6}$$

A detailed comparison of the experimental results from Camoin et al. [62] with the theory is not possible, because data for the surface tension, contact angle and the contact line radius are not given in Ref. [62].

Both attractive and repulsive lateral immersion forces between two vertical cylinders, as well as between a vertical cylinder and a wall, were obtained by Velev et al. [64] by means of a piezo-transduser balance, see Fig. 4. One of the cylinders ('1' in Fig. 4) is connected by a thin glass needle to a piezo-resistive sensor; thus the sensor can detect the pressure caused by the needle, which is in fact the horizontal component of the force exerted on the vertical cylinder 1. The other cylinder 2 can be moved during the experiment in order to change the distance L between the bodies. Fig. 5 presents the dimensionless capillary force $F/(q\sigma Q_1 Q_2)$ vs. the dimensionless distance qL measured by Velev et al. [64]. The liquid is pure water, $\sigma = 72.4$ mN/m, $q^{-1} = 2.72$ mm; the two cylinders are hydrophilic, so $\psi_1 = \psi_2 = 90°$; the radii of the cylinders are $r_1 = 370$ μm and $r_2 = 315$ μm. The solid curve in Fig. 5 is drawn by means of Eq. (2.1) without using any adjustable parameters. One sees that Eq. (2.1) agrees well with the experiment except in the region of small distances, where the asymptotic formula Eq. (2.1), derived under the assumption for small meniscus slope and long distances, is no longer valid.

Systematic measurements of lateral immersion force between two vertical cylin-

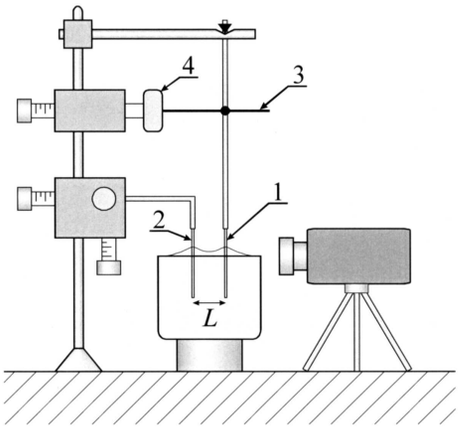

Fig. 4. Sketch of the experimental setup used in Velev et al. [64] to measure the capillary immersion force between two vertical cylinders, '1' and '2'; '3' is a glass needle, which transfers the horizontal force exerted on cylinder '1' to a piezo-resistive sensor '4'. Thus the force, converted into electric signal, is measured as a function of the distance L.

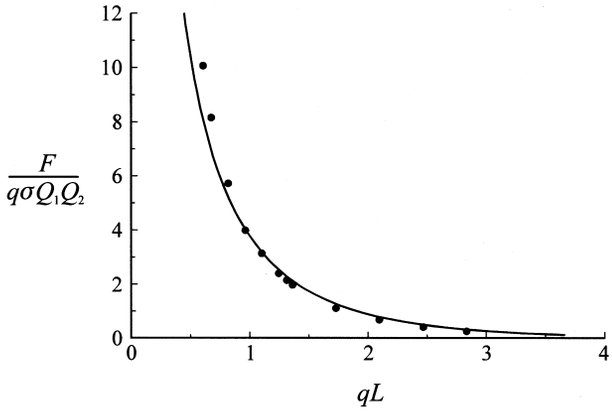

Fig. 5. Force F of capillary attraction between two hydrophilic vertical cylinders measured in Velev et al. [64] by means of the piezo-transducer balance sketched in Fig. 4; F is plotted vs. the distance L between the axes of the cylinders, the parameters values are $q^{-1} = 2.72$ mm, $\sigma = 72.4$ mN/m, $Q_1 = 0.370$ mm, $Q_2 = 0.315$ mm. The solid line is calculated by means of Eq. (2.1); no adjustable parameters

ders, between cylinder and sphere, and between sphere and vertical wall were carried out in Dushkin et al. [65,66] by means of a torsion micro-balance, see Fig. 6. The latter in principle resembles the balance used by H. Cavendish to measure the gravitational constant in 1798,[1] but is much smaller. The force between two couples of vertical cylinders and/or spheres (Fig. 6) was measured by counterbalancing the moment created by the two couples of forces with the torsion moment of a fine platinum wire, whose diameter was 10 μm and 25 μm in different experiments. The angle of torsion, φ, was measured by reflection of a laser beam from a mirror attached to the anchor of the balance, see Fig. 6. Fig. 7 shows data from Dushkin et al. [65] for the capillary force between two identical vertical cylinders for $r_1 = r_2 = 50$, 165 and 365 μm; the solid lines in Fig. 7 are calculated by means of Eq. (2.1) without using any adjustable parameter. It is seen that the theory and experiment agree well in the range of validity of the theoretical expressions. At shorter distances between the two interacting bodies, at which the linearized theory is not accurate, deviations from Eq. (2.1) are experimentally detected [66], as it could be expected.

The lateral capillary force between two freely floating particles (no attachment to any holders) is more difficult to be measured. One way is to counterbalance the capillary force by the gravity force in the vicinity of an inclined meniscus, see Fig. 6 in Velev et al. [23]. Other way is to measure the displacement of a floating particle (moving under the action of the lateral flotation force) as a function of time; knowing the surface drag coefficient one can determine the capillary force, and vice versa, see Petkov et al. [68] and the next Section 2.3.

[1]About the measurement of the gravitational constant see Rose et al. [67].

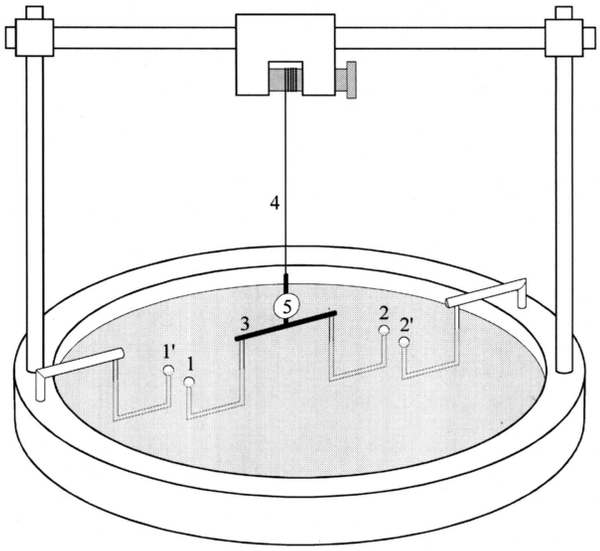

Fig. 6. Sketch of a torsion balance, used by Dushkin et al. [65,66] to measure the capillary attraction between two pairs of small glass spheres ($1 - 1'$ and $2 - 2'$) attached to holders. The immersed part of the holders is shown dashed. One of the particles in each pair (these are particles 1 and 2) is connected to the central anchor 3, which is suspended on a platinum wire 4; the angle of torsion is measured by reflection of a light beam from the mirror 5.

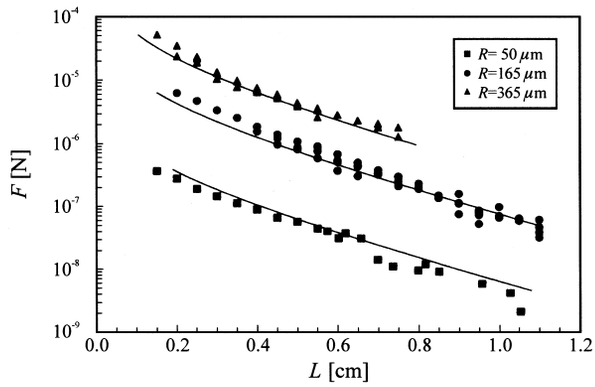

Fig. 7. Plot of the force of capillary attraction F vs. the distance L between the axes of two identical vertical cylinders of radius R. The force is measured by Dushkin et al. [65,66] by means of the torsion balance shown in Fig. 6; the three curves correspond to cylinders of radii $R = 50$, 165 and 365 μm. The solid lines are drawn by means of Eq. (2.1); no adjustable parameters.

2.3. Particle–wall interactions, capillary image forces and their application

The overlap of the meniscus around a floating particle with the meniscus on a vertical wall gives rise to a particle–wall interaction, which can be both repulsive and attractive. Imagine a floating spherical particle in the vicinity of a vertical planar wall. We will use subscripts '1' and '2' to denote parameters characterizing the wall and particle, respectively. First, following Kralchevsky et al. [22], we consider the simplest case, when the contact angle at the wall is $\alpha_1 = 90°$. In such a case the meniscus would be flat if the floating particle (Fig. 8a) were removed. Let us denote by $\zeta_0(x,y)$ the meniscus shape in the presence of particle. Since $\alpha_1 = 90°$ the function $\zeta_0(x,y)$ must satisfy the boundary condition $(\partial\zeta_0/\partial x)_{x=0} = 0$ at the wall surface. Using considerations for symmetry one realizes that the meniscus shape $\zeta_0(x,y)$ in Fig. 8a would be the same if (instead of a wall at a distance s) one has a second particle (mirror image) floating at a distance $2s$ from the original one. The 'image' must be identical to the original particle with respect to its size, weight and contact angle, that is the particle and its image ought to have identical capillary charges, Q_2. Note, that the capillary charge of a floating particle is given by the expression [20]

$$Q_2 \approx \frac{1}{6}q^2R_2^3(2 - 4D_2 + 3\ \cos\alpha_2 - \cos^3\alpha_2)(1 + O(qR_2)), \quad D_2 \equiv \frac{\rho_2 - \rho_{II}}{\rho_I - \rho_{II}} \tag{2.7}$$

where R_2, α_2 and ρ_2 are the radius, contact angle and the mass density of the particle; ρ_I and ρ_{II} are respectively the mass densities of the lower and upper fluid phases. As mentioned previously, for two identical particles the lateral capillary force is always attractive. Hence, the particle and its mirror image depicted in Fig. 8a will attract each other, which in fact means that the wall will attract the floating particle; the resulting force will (asymptotically) obey Eq. (2.1) with $Q_1 = Q_2$.

The boundary condition $\zeta_0(x = 0) = 0$ represents a requirement for a zero elevation of the contact line at the wall. As noticed in Ref. [22] this can be realized in practice if the contact line is attached to the edge of a vertical plate, as shown in Fig. 8b, or to the boundary between a hydrophobic and a hydrophilic domain on the wall. Using again considerations for symmetry one realizes that the meniscus shape $\zeta_0(x,y)$ in Fig. 8b would be the same if (instead of a wall at a distance s) one has a second particle (image) of the *opposite* capillary charge ($Q_1 = -Q_2$) at a distance $2s$ from the original particle. In such a case the capillary force is repulsive, i.e. in reality the wall will repel the floating particle [22].

The configuration with repulsive capillary image force, which is depicted in Fig. 8b, is realized experimentally by Velev et al. [23] and Petkov et al. [68] as shown in Fig. 9. In these experiments the 'wall' is a hydrophobic Teflon barrier, whose position along the vertical can be precisely varied and adjusted. The total lateral capillary force exerted on the particle depicted in Fig. 9 is given by the following

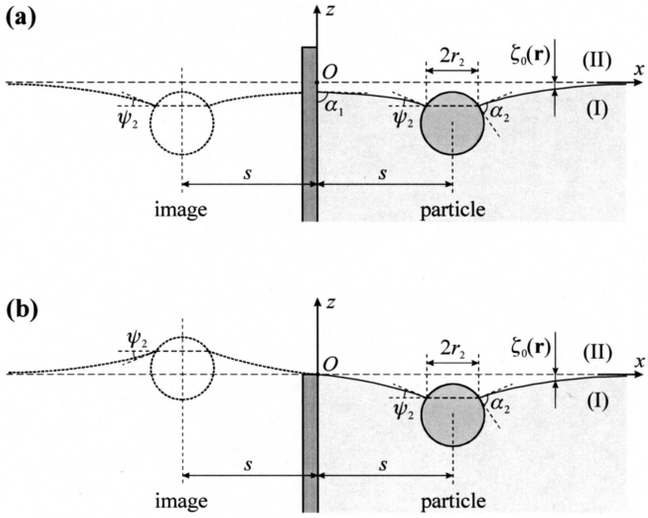

Fig. 8. Sketch of the meniscus profile, $\zeta_0(\mathbf{r})$, around a particle floating in the vicinity of a vertical wall; α_2 and r_2 are the particle contact angle and contact line radius; ψ_2 is the meniscus slope angle at the particle contact line; (a) fixed contact angle at the wall ($\alpha_1 = 90°$) corresponding to attractive capillary image force; (b) fixed contact line at the wall ($\zeta_0 \equiv 0$ for $x = 0$) which leads to repulsive capillary image force [22].

asymptotic expression [22]:

$$F(s) \approx \pi\sigma\left[2Q_2qHe^{-qs} + q(r_2qHe^{-qs})^2 - 2qQ_2^2K_1(2qs)\right]\left(1 + O(q^2R_2^2)\right) \times (r_2 \ll s) \tag{2.8}$$

Here H characterizes the position of the contact line on the wall with respect to the non-disturbed horizontal liquid surface (Fig. 9); s is the particle–wall distance; and q is defined by Eq. (2.3) (thick films). The first term in the right-hand side of Eq. (2.8) expresses the gravity force pushing the particle to slide down over the inclined meniscus on the wall; the second term originates from the pressure difference across the meniscus on the wall — this pressure difference also pushes the particle to slide downward, toward the wall; the third term expresses the repulsive 'capillary image force', that is the particle is repelled by its mirror image with respect to the wall surface, as it is in Fig. 8b.

Note that for the configuration in Fig. 9 the first two terms in Eq. (2.8) are positive, whereas the third one is negative. For each given H there will be a distance $s = s^*$, for which $F(s^*) = 0$. This distance corresponds to an equilibrium position of the particle, i.e. one can expect that a particle floating in a vicinity of the vertical wall (Fig. 9) at equilibrium will stay at a distance s^* from the wall. The measurements carried out by Velev et al. [23] show that really this is the experimental situation. Varying H one can change the distance s^*. Fig. 10 shows experimental points for H vs. s^* measured with a hydrophobized copper bead floating on the surface of pure water. The radius of the bead is $R_2 = 700 \pm 15$ μm and its contact angle with pure water is $\alpha_2 = 100°$. The accuracy and the repro-

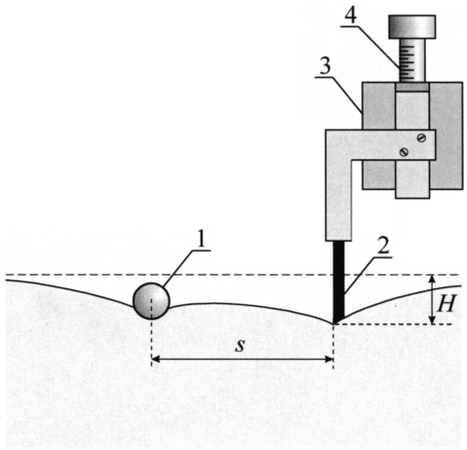

Fig. 9. Experimental setup used for studying capillary interactions [23], for measurement of surface drag coefficient [68] and surface shear viscosity of surfactant adsorption monolayers [72]. Particle 1 is floating at a distance s from a hydrophobic plate 2, whose lower edge is located at a distance H below the level of the non-disturbed horizontal liquid; H can be varied by means of the micrometric table 3 and screw 4.

ducibility of the measurement are about ± 2 μm for H and ± 20 μm for s^*. The theoretical curve (the dashed line in Fig. 10) is drawn with $R_2 = 711$ μm which agrees well with the optically measured radius of the bead; a more rigorous expression derived by Velev et al. [23] is used in the calculations, instead of the asymptotic formula Eq. (2.8). One sees in Fig. 10 that the agreement between theory and experiment is very good.

As demonstrated by Petkov et al. [68], knowing the capillary force F, see Eq. (2.8), and measuring the particle velocity, $\dot{s}$in dynamic experiments one can

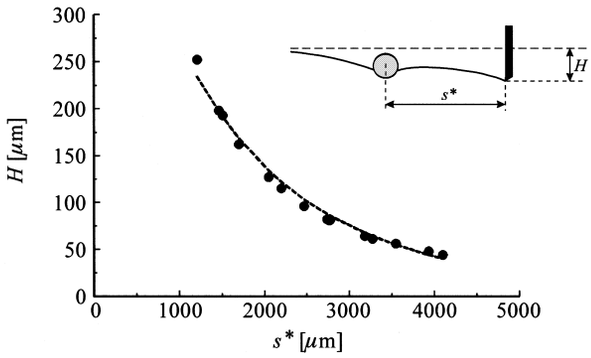

Fig. 10. Experimental data (●) from Velev et al. [23] for the dependence of H on the equilibrium distance s^* for a hydrophobized copper sphere, see the text for the notation. The dashed line represents the theoretical dependence calculated with the experimental values of the contact angle $\alpha_2 = 100°$ and sphere radius $R_2 = 711$ μm.

determine the drag force, F_d:

$$F_d = F - m\ddot{s}, \quad F_d \equiv 6\pi\eta R_2 f_d \dot{s} \tag{2.9}$$

where R_2, m and $\ddot{s}$ are the particle radius, mass and acceleration, η is the viscosity of the liquid and f_d is the drag coefficient. If the particle were entirely immersed in the bulk liquid, F_d would be given by the Stokes formula, $F_d = 6\pi\eta R_2 \dot{s}$, and f_d would be equal to 1. In general, f_d differs from unity because the particle is attached to the interface and protrudes from the underlying liquid phase. An example is given in Fig. 11, where the experimentally measured velocity $\dot{s}$ of a particle approaching the wall is plotted vs. the capillary force $F(s)$, calculated by means of Eqs. (2.7) and (2.8) for the experimental values of the distance s. The particle is a glass sphere of radius $R_2 = 229$ μm and contact angle $\alpha_2 = 48.7°$ floating at the surface of pure water, $\sigma = 72$ mN/m. The straight line in Fig. 11 corresponds to drag force equal to the capillary force, i.e. $F_d = F(s)$; from the slope of the straight line one determines $f_d = 0.68$. The deviation of the data for the larger $F(s)$ is not a discrepancy between theory and experiment: the deviation is due to the inertia term in Eq. (2.9), $m\ddot{s}$ which is not negligible for shorter distances between the particle and wall, at which the approximation $F_d \approx F(s)$ is not good enough.

According to the hydrodynamic theory by Brenner and Leal [69,70], and Danov et al. [71], the drag coefficient f_d of a particle attached to a planar fluid interface is a function only of the viscosities of the two fluids and of the three-phase contact angle, α_2. The experiment by Petkov et al. [68] gives f_d varying between 0.68 and 0.54 for particle contact angle varying from 49° to 82° (the less the depth of particle immersion, the less the drag coefficient, as could be expected); the data are in a

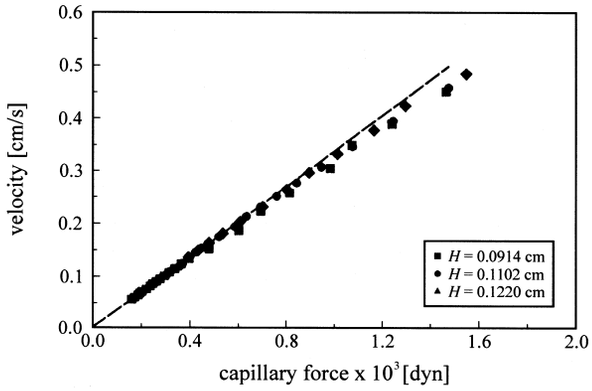

Fig. 11. Experimental data from Petkov et al. [68] for the velocity $\dot{s}$ of a glass sphere plotted vs. The capillary force F calculated from Eq. (2.8); the sphere is floating (see Fig. 9) on the surface of pure water. The slope of the dashed line, drawn in accordance with Eq. (2.9) (the inertial term $m\ddot{s}$ neglected), gives drag coefficient $f_d = 0.68$. the data are obtained in three runs corresponding to three fixed values of H denoted in the figure.

very good quantitative agreement with the hydrodynamic theory of the drag coefficient [69–71].

If the floating particle is heavy enough, it deforms the surrounding liquid surface; the deformation travels together with the particle thus increasing f_d several times [68]; so far there is no quantitative hydrodynamic theory of the latter effect. The addition of surfactant strongly increases f_d. The latter effect has been used in Petkov et al. [72] to measure the surface viscosity of adsorption monolayers from low molecular weight surfactants, which exhibit fast kinetics of adsorption. For these surfactants the surface viscosity is too low to be accessible to the conventional experimental methods. However, the motion of a sphere of radius 200–300 μm turns out to be sensitive to the friction within the adsorption layer (thick no more than 2 nm) of surfactants such as sodium dodecyl sulfate (SDS) and hexadecyl-trimethyl-ammonium-bromide (HTAB). To demonstrate that, in Fig. 12 we present experimental data from Petkov et al. [72] for the velocity of a particle (Fig. 9) plotted vs. the capillary force $F(s)$, calculated by means of Eq. (2.7) and Eq. (2.8). One sees (Fig. 12) that again the data for $\dot{s}$ vs. $F(s)$ comply with straight lines, whereas the plots of $\dot{s}$ vs. time t are non-linear (the inset in Fig. 12). From the slopes of the straight lines in Fig. 12 the drag coefficient f_d was determined; the obtained values of f_d are also shown in Fig. 12. Note, that the addition of surfactant increases f_d from 0.66 up to 1.6. This effect, converted in terms of surface viscosity, gives $\eta_s = 1.5$ and 2.0×10^{-6} kg/s for the surface viscosity of dense SDS and HTAB adsorption monolayers, respectively [72].

Note that if the kinetics of surfactant adsorption is not fast enough to damp the surface elastic effects, the drag coefficient f_d can be influenced not only by the

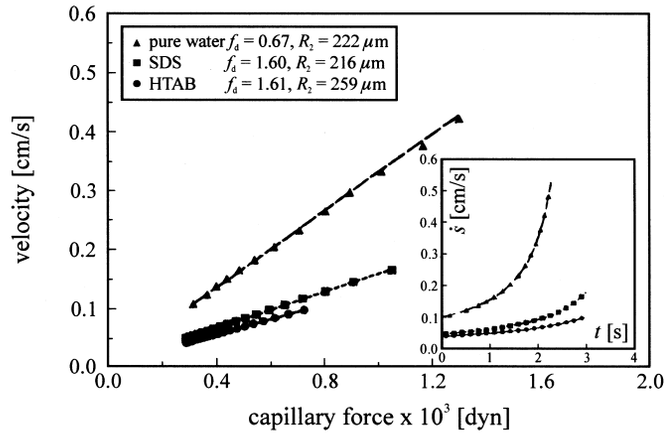

Fig. 12. Experimental data from [72] for the velocity $\dot{s}$ of floating glass spheres plotted vs. the capillary force F calculated from Eq. (2.8). The slope of each experimental line gives the value of the surface drag coefficient, f_d. Data about the type of the solution, the determined f_d and the particle radius R_2 are given in the figure. The inset shows the experimental plot of $\dot{s}$ (cm/s) vs. time (s), which becomes linear when plotted as $\dot{s}$ vs. F.

surface viscosity, but also by the surface (Gibbs) elasticity. The complete dynamic problem, involving the effects of surface viscosity, surface elasticity and dynamics of surfactant adsorption has not yet been solved theoretically.

3. Energy approach to the lateral capillary interactions

Having reviewed the experiments on capillary forces let us come back to the theory. Our purpose below is to give the derivation of the most popular asymptotic formula for the lateral capillary forces, Eq. (2.1), and to demonstrate that this equation is applicable to both flotation and immersion forces, with particles attached to single interfaces or confined in thin liquid films, see Fig. 1. The cause of the capillary interaction is the overlap of the deformations around such two particles. Hence, the key to the theoretical description of this interaction is to solve the Laplace equation, governing the meniscus shape, for a given configuration of particles at an interface or in a thin film.

3.1. The linearized Laplace equation for fluid interfaces and thin films

Let $z = \zeta(x,y)$ be the equation of the deformed fluid interface. The interfacial shape obeys the Laplace equation of capillarity [73]

$$\nabla_{\mathrm{II}} \cdot \left(\frac{\nabla_{\mathrm{II}} \zeta}{\sqrt{1 + |\nabla_{\mathrm{II}} \zeta|^2}} \right) = [P_{\mathrm{II}}(\zeta) - P_{\mathrm{I}}(\zeta)]/\sigma \tag{3.1}$$

$$\nabla_{\mathrm{II}} = e_x \frac{\partial}{\partial x} + e_y \frac{\partial}{\partial y} \tag{3.2}$$

see also Finn [74] and Kralchevsky et al. [75]. Here ∇_{II} is the two-dimensional gradient operator in the plane xy. Note that Eq. (3.1) is expressed in a covariant form and can be specified for any type of curvilinear coordinates in the plane xy (not only Cartesian ones). The pressures P_{I} and P_{II} on the two sides of the interface can be dependent on ζ because of the effects of hydrostatic pressure and disjoining pressure, see below.

As an example, let us consider a spherical particle which is entrapped into a wetting liquid film, Fig. 13. The upper surface of the liquid film is planar far from the particle; this plane is chosen to be the level $z = 0$ of the coordinate system. The thickness of the plane-parallel liquid film far from the particle is h_0. The pressure inside and outside the film (in phases I and II) can be expressed in the form [14,21,76,77]:

$$P_{\mathrm{I}}(\zeta) = P_{\mathrm{I}}^{(0)} - \rho_{\mathrm{I}} g\zeta + \Pi(h_0 + \zeta), \quad P_{\mathrm{II}}(\zeta) = P_{\mathrm{II}}^{(0)} - \rho_{\mathrm{II}} g\zeta, \quad |\nabla_{\mathrm{II}}\, \zeta|^2 \ll 1 \tag{3.3}$$

Here g is the acceleration due to gravity, ρ_{I} and ρ_{II} are the mass densities in phases I and II, $P_{\mathrm{I}}^{(0)}$ and $P_{\mathrm{II}}^{(0)}$ are the pressures in the respective phases at the level $z = 0$; Π is the disjoining pressure, which depends on the local thickness of the wetting film. The terms $\rho_{\mathrm{I}} g\zeta$, and $\rho_{\mathrm{II}} g\zeta$, express hydrostatic pressure, which is predominant in thick films, i.e. for $h_0 \geq$ 100 nm, in which the disjoining pressure Π (the interaction of the two adjacent phases across the liquid film) becomes negligible. In fact, it is the gravity which keeps the interface planar far from the particle when the film is *thick*. On the contrary, when the film is *thin*, the existence of a positive disjoining pressure (repulsion between the two film surfaces) keeps the film plane–parallel far from the particle. The condition for stable mechanical equilibrium of this film is

$$P_{\mathrm{II}}^{(0)} = P_{\mathrm{I}}^{(0)} + \Pi(h_0), \quad \Pi' \equiv \left(\frac{\partial \Pi}{\partial h}\right)_{h=h_0} < 0 \tag{3.4}$$

see e.g. Kralchevsky [61]. Expanding the disjoining pressure term in Eq. (3.3) in series one obtains

$$\Pi(h_0 + \zeta) = \Pi(h_0) + \Pi'\zeta + \ldots \tag{3.5}$$

Usually the slope of the meniscus around particles, like that depicted in Fig. 13, is small enough and the approximation $|\nabla_{\mathrm{II}}\zeta|^2 \ll 1$ can be applied. Then combining Eqs. (3.1)–(3.5) one obtains a linearized form of Laplace equation:

$$\nabla_{\Pi}^2\zeta = q^2\zeta, \quad q^2 \equiv \frac{\Delta\rho g}{\sigma} + \frac{-\Pi'}{\sigma} \quad (\Delta\rho \equiv \rho_{\mathrm{I}} - \rho_{\mathrm{II}}; |\nabla_{\mathrm{II}}\zeta|^2 \ll 1) \tag{3.6}$$

Note that $\Pi' < 0$. The disjoining pressure effect is negligible when the film is thick enough to have $-\Pi'(h_0) \ll \Delta\rho g$. In the latter case the upper film surface behaves as a single interface (it does not 'feel' the lower film surface). The quantity q^{-1} is a characteristic capillary length, which determines the range of action of the lateral capillary forces. In thick films (Π' is negligible) $q^{-1}$is of the order of millimeters, e.g. $q^{-1} = 2.7$ mm for water–air interface. However, in thin films (Π' is predominant) q^{-1}can be of the order of 10–100 nm, see Kralchevsky et al. [21].

3.2. Flotation force: energy approach in superposition approximation

The simpler derivation of Eq. (2.1), based on energy considerations, was given by Nicolson [3] long ago for floating particles. Following his approach let us consider a floating spherical particle of mass m_i, which creates an interfacial deformation, see Fig. 14. For a single particle Eq. (3.6), written in cylindrical coordinates, reduces to the modified Bessel equation, whose solution (for small meniscus slope) has the form [78]:

$$\zeta_i(r) = r_i \sin\psi_i \mathrm{K}_0(qr) = Q_i \mathrm{K}_0(qr) \quad (i = 1,2) \tag{3.7}$$

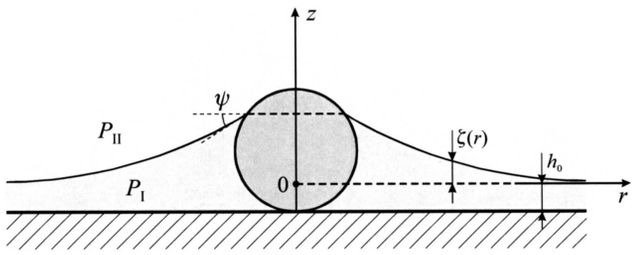

Fig. 13. Colloidal sphere partially immersed in a liquid layer on a substrate; $\zeta(r)$ describes the shape of the meniscus formed around the sphere; P_I and P_{II} are the pressures inside the liquid layer and in the upper fluid phase; h_0 is the thickness of the non-disturbed liquid layer; the latter is kept plane-parallel by the gravity, when the layer is thick, and by a repulsive disjoining pressure when the film is thin.

where r_i is the contact line radius and ψ_i is the meniscus slope angle at the contact line, and Eq. (2.2) has been used; K_0 is the Macdonald (modified Bessel) function of zero order, see Janke et al. [58], Abramowitz et al. [59], Korn and Korn [60].

The force due to gravity, $F_{g(i)}$, which is exerted on the i-th particle ($i = 1,2$) is counterbalanced by the vertically resolved surface tension force, acting per unit length of the three-phase contact line:

$$F_{g(i)} = 2\pi\sigma r_i \sin\psi_i 2\pi\sigma Q_i \quad (i = 1,2) \tag{3.8}$$

cf. Fig. 14 and Eq. (2.2). Here $F_{g(i)} = m_i g - F_b$ with F_b being the buoyancy (Archimedes) force; expression for F_b for floating particles can be found in Ivanov and Kralchevsky [79].

Now let us consider particle 2 situated at a horizontal distance L from particle 1. Following Nicolson [3] we assume that due to the meniscus created by particle 1,

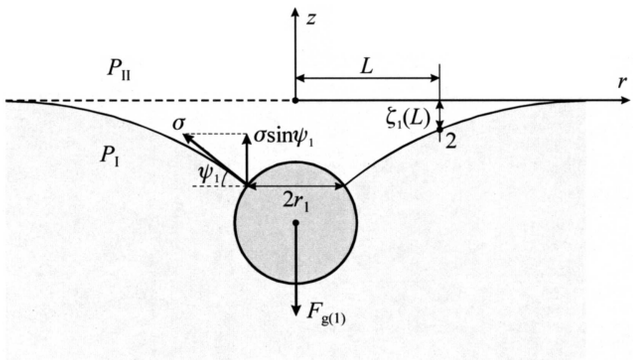

Fig. 14. A heavy spherical particle creates a concave meniscus on an otherwise horizontal fluid interface of tension σ, $F_{g(1)}$ is the net force due to gravity (a combination of particle weight and buoyancy); ψ_1 is the meniscus slope at the particle contact line of radius r_1.

the mass-center of particle 2 is situated at a distance $\zeta_1(L)$ below the horizontal plane $z = 0$, see point 2 in Fig. 14. The work carried out by the gravitational force to bring particle 2 from level $z = 0$ down to level $z = -\zeta_1(L)$ is [3,17]

$$\Delta W_g = -F_{g(2)}\zeta_1(L) = -2\pi\sigma Q_1 Q_2 \mathrm{K}_0(qL) \tag{3.9}$$

where at the last step Eqs. (3.7) and (3.8) have been used. Having in mind that

$$F = -\frac{d\Delta W_g}{dL}; \quad \frac{d\mathrm{K}_0(x)}{dx} = -\mathrm{K}_1(x) \tag{3.10}$$

one easily obtains Eq. (2.1) differentiating Eq. (3.9). This derivation of Eq. (2.1) makes use of many approximations, the most obvious of them being $|\nabla_{\mathrm{II}}\zeta|^2 \ll 1$ and $r_i \ll L$. In particular, it has been implicitly assumed that for $r_i \ll L$ $(i = 1,2)$ the meniscus shape is a superposition of the axisymmetric menisci around each particle in isolation, described by Eq. (3.7). These and other approximations are discussed in Section 3.4, where a more general formulation of the energy approach can be found.

3.3. Immersion force: energy approach in superposition approximation

Let us consider a couple of vertical cylinders, each of them being immersed partially in Phase I, and partially in Phase II. For each of these cylinders in isolation (Fig. 15) the shape of the surrounding capillary meniscus is given by Eq. (3.7). The contact angle α_i at the three phase contact line of the i-th cylinder $(i = 1,2)$ obeys the Young equation:

$$\sigma_{i,\mathrm{II}} - \sigma_{i,\mathrm{I}} = \sigma\cos\alpha_i = \sigma\sin\psi_i = \sigma Q_i/r_i \quad (i = 1,2) \tag{3.11}$$

cf. Fig. 15 and Eq. (2.2). Here $\sigma_{i,\mathrm{I}}$ and $\sigma_{i,\mathrm{II}}$ are surface free energies per unit area of the boundary of the i-th cylinder with Phases I and II, respectively. The two cylinders are assumed immobile in vertical direction.

Let us assume that Cylinder 1 is fixed at the z-axis (Fig. 15) and let us consider a process in which the vertical Cylinder 2 is moved in horizontal direction from infinity to some finite distance L $(L \gg r_1, r_2)$. At such a distance L the level of the liquid meniscus around cylinder 1 rises with $\zeta_1(L)$, see Fig. 15. Thus the surface area of cylinder 2 wet by Fluid 1 increases, whereas the area wet by Fluid 2 decreases. As a result, the energy of wetting of cylinder 2 will change with

$$\Delta W_w \approx -2\pi r_2\zeta_1(L)(\sigma_{2,\mathrm{II}} - \sigma_{2,\mathrm{I}}) = -2\pi\sigma Q_1 Q_2 K_0(qL) \tag{3.12}$$

where at the last step Eqs. (3.7) and (3.11) have been used. Finally, identifying the capillary force with the derivative of the wetting energy, $F = -d\Delta W_w / dL$, one easily obtains Eq. (2.1) differentiating Eq. (3.12). This derivation of Eq. (2.1) makes use of the approximations $r_i \ll L$, $|\nabla_{\mathrm{II}}\zeta|^2 \ll 1$, and the superposition approximation. In the case of spherical particles the variation in the position of the contact

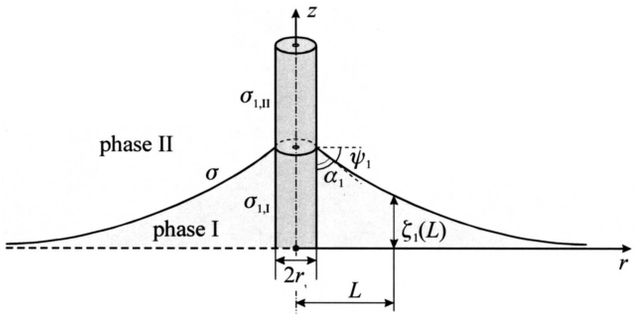

Fig. 15. A vertical cylinder (rod) of radius r_1 creates a convex meniscus on an otherwise horizontal fluid interface of tension σ, the boundaries of the cylinder with the phases I and II have solid-fluid surface tensions $\sigma_{1,I}$ and $\sigma_{1,II}$; α_1 is the three-phase contact angle; ψ_1 is the meniscus slope at the particle contact line.

line on the particle surface is accompanied with a variation of the contact line radii, r_1 and r_2, and of the slope angles ψ_1 and ψ_2; these effects are taken into account in Kralchevsky et al. [14,18–20,22,24].

In spite of being approximate, the derivations of the expression for F, which are presented in Sections 3.2 and 3.3, clearly demonstrate the difference between the physical origin of the flotation and immersion forces. Indeed, the flotation force is defined as a derivative of the gravitational energy W_g, see Eq. (3.9), whereas the immersion force is equal to the derivative of the wetting energy W_w, see Eq. (3.12).

3.4. General expression for the grand thermodynamic potential

The grand thermodynamic potential of a system of N particles attached to the interface between phases I and II can be written in the form [14,20,21]:

$$\Omega(\mathbf{r}_1,\ldots,\mathbf{r}_N) = W_g + W_w + W_m + \text{const.} \tag{3.13}$$

$$W_g = \sum_{i=1}^{N} m_i g Z_i^{(c)} - \sum_{Y=\text{I,II}} \int_{V_Y} P_Y dV \tag{3.14}$$

$$W_w = \sum_{i=1}^{N} \sum_{Y=\text{I,II}} \sigma_{iY} A_{iY}, \quad W_m = \sigma A, \tag{3.15}$$

where $\mathbf{r}_1$, $\mathbf{r}_2$,...,$\mathbf{r}_N$ are the position vectors of the particle mass centers and m_i (i = 1,2,...,N) are the masses of the particles, $Z_i^{(c)}$ is the projection of $\mathbf{r}_i$ along the vertical, P_Y and V_Y (Y = I, II) are pressure and volume of the Y-th fluid phase; σ and A are the interfacial tension and the area of the boundary (the meniscus) between fluid phases I and II; A_{iY} and σ_{iY} are area and the surface free energy density of the boundary between particle 'i' and phase 'Y'; the additive constant in Eq. (3.13) does not depend on $\mathbf{r}_1$, $\mathbf{r}_2$,...,$\mathbf{r}_N$; W_g, W_w and W_m are respectively the

gravitational, wetting and meniscus contribution to the grand potential Ω. Then the lateral capillary force between particles 1 and 2 is determined by differentiation:

$$F^{(12)} = -\frac{\partial \Omega}{\partial r_{12}}, \quad r_{12} = |\mathbf{r}_1 - \mathbf{r}_2| \tag{3.16}$$

When the distance between two particles varies, the shape of the meniscus between phases I and II (and consequently W_m) alters; during the same variation the areas of the particle surfaces wet by phases I and II also vary, which leads to a change in W_w; last but not least, the change in the meniscus shape is accompanied by changes in the positions of the mass centers of particles and fluid phases, which gives rise to a variation in their gravitational energy accounted for by W_g. Eqs. (3.13)–(3.16) are applicable also to thin films; one should take into account the fact that in such a case the meniscus surface tension depends on the local thickness of the film, $\sigma = \sigma(\zeta)$, so that [21,80]

$$\frac{d\sigma}{d\zeta} = -\left(1 + |\nabla_{\Pi}\zeta|^2\right)^{1/2}\Pi \quad \text{(thin films)} \tag{3.17}$$

where, as usual, Π is the disjoining pressure. In other words, the disjoining pressure effect is 'hidden' in the meniscus energy term, W_m, in Eq. (3.13).

The explicit form of Eqs. (3.14) and (3.15), and the relative importance of W_g, W_w and W_m, depend on the specific configuration of the system. For example, in the case of small floating particles at separations $L \gg r_1, r_2$, it turns out that $W_m \approx -W_g/2 - W_w$ and then $\Omega = W_g + W_w + W_m \approx W_g/2 \approx \Delta W_g$, where ΔW_g is given by the Nicolson's expression, Eq. (3.9).

In the framework of the *energy* approach the treatment of flotation and immersion lateral capillary forces is different, insofar as in the former case Ω is dominated by W_g, whereas in the latter case Ω is dominated by W_w, cf. Sections 3.2 and 3.3. On the other hand, there is an equivalent *force* approach (considered in Section 4) which provides an unified description of the flotation and immersion forces.

3.5. Interactions at fixed slope and fixed elevation

In some cases the distance between two particles attached to an interface can decrease at constant values of the slope angle ψ_i and contact radius r_i ($i = 1,2$). In such a case the capillary charge $Q_i = r_i \sin\psi_i$ is also constant. A typical example is the capillary interaction between two vertical cylinders (rods) of radii r_i and contact angles $\alpha_i = \pi/2 - \psi_i$ ($i = 1,2$). Other example is the capillary interaction between small floating particles, for which it can be proven [20] that they approach each other at (approx.) constant capillary charge Q_i. In all these cases the average elevation of the contact line,

$$h_i(L) \equiv \frac{1}{2\pi r_i}\oint_{c_i} dl\zeta, \tag{3.18}$$

depends on the distance L between the two particles; here C_i denotes the projection of the contact line on the horizontal plane xy. The following expression for the interaction energy $\Delta\Omega$ has been derived for such cases [14,19,20]:

$$\Delta\Omega(L) \approx -\pi\sigma \sum_{i=1,2} Q_i[h_i(L) - h_{i\infty}] \quad (\psi_i = \text{const.}, r_i = \text{const.}) \tag{3.19}$$

where $h_{i\infty} = h_i(L \to \infty)$.

In other cases, like that depicted in Fig. 3, the elevation of the contact line, h_i, remains constant when the particles approach each other. In such cases the average meniscus slope of the contact line,

$$\sin\Psi_i(L) \equiv \frac{1}{2\pi r_i}\oint_{c_i} dl\tilde{\mathrm{n}} \cdot \nabla_{\mathrm{II}}\zeta, \tag{3.20}$$

depends on the distance L between the two particles; here $\tilde{\mathbf{n}}$ is a running outer unit normal to the contour C_i. The following expression for the interaction energy $\Delta\Omega$ has been derived for the latter case [21,25]:

$$\Delta\Omega(L) \approx \pi\sigma \sum_{i=1,2} h_i r_i[\sin\Psi_i(L) - \sin\Psi_{i\infty}] \quad (h_i = \text{const.}, \ r_i = \text{const.}) \tag{3.21}$$

where $\Psi_{i\infty} = \Psi_i(L \to \infty)$. To calculate the capillary force from Eqs. (3.19) or (3.21) one is to first solve the Laplace equation, along with the respective boundary conditions, and then to determine $h_i(L)$ or $\Psi_i(L)$ by means of Eqs. (3.18) or (3.20). Note also that Eqs. (3.19) and (3.21) are valid for small meniscus slope, $|\nabla_{\mathrm{II}}\zeta|^2 \ll 1$.

4. Force approach to the lateral capillary interactions

4.1. Integral expressions for the capillary force

In the force approach (which is alternative to the energy approach from Section 3) the lateral capillary force exerted on each of the interacting particles is calculated by integrating the meniscus interfacial tension $\boldsymbol{\sigma}$ along the contact line and the hydrostatic pressure P throughout the particle surface [18–21]:

$$\mathbf{F}^{(i)} = \mathbf{F}^{(i\sigma)} + \mathbf{F}^{(ip)}, \qquad i = 2, \ldots, \tag{4.1}$$

where the contribution of interfacial tension is

$$\mathbf{F}^{(i\sigma)} \equiv \mathbf{U}_{\mathrm{II}} \cdot \oint_{L_i} dl\mathbf{m}\sigma \tag{4.2}$$

and the contribution of the hydrostatic pressure is

$$\mathbf{F}^{(ip)} \equiv \mathbf{U}_{\mathrm{II}} \cdot \oint_{S_i} ds(-\mathbf{n}P) \tag{4.3}$$

Here $\mathbf{U}_{\mathrm{II}}$ is the unit operator (tensor) of the horizontal plane xy; in Eqs. (4.2) and (4.3) this operator projects the respective vectorial integrals onto the xy-plane; L_i denotes the three phase contact line on the particle surface (Fig. 16) and dl is a linear element; $\mathbf{m}$ is an outer running unit normal to the contact line; the vector $\mathbf{m}$ is also tangential to the meniscus surface and has the direction of the surface tension force exerted on the particle along the contact line. Likewise, S_i denotes the particle surface with outer unit running normal $\mathbf{n}$; ds is a scalar surface element; the vector '$-\mathbf{n}$' has the direction of the outer pressure exerted on the surface of each particle. In Refs. [18,19,21] it has been proven, that the integral expressions (Eqs. (4.1), (4.2) and (4.3)) are compatible with the Newton's third law, i.e. $\mathbf{F}^{(1)} = -\mathbf{F}^{(2)}$, as it must be.

Note that the interfacial bending moment can also contribute to the lateral capillary force, see Kralchevsky et al. [25] and Eq. (6.16) below, although this contribution is expected to be important only for interfaces and membranes of low tension σ.

As an example, let us consider two particles entrapped in a liquid film on a substrate, see Fig. 16. If the contact lines L_1 and L_2 were horizontal, the integrals in Eqs. (4.2) and (4.3) would be equal to zero because of the symmetry of the force distributions. However, due to the overlap of the interfacial perturbations created by each particle, the contact lines are slightly inclined, which is enough to break the symmetry of the force distribution and to give rise to a non-zero net (integral) force exerted on each of the two particles.

The existence of inclination of the contact line can be clearly seen in Fig. 17, which represents three photographs of thin vertical glass rods partially immersed in water; the photographs have been taken Velev et al. [64] with the experimental setup sketched in Fig. 4. One sees that the contact line on an isolated rod is

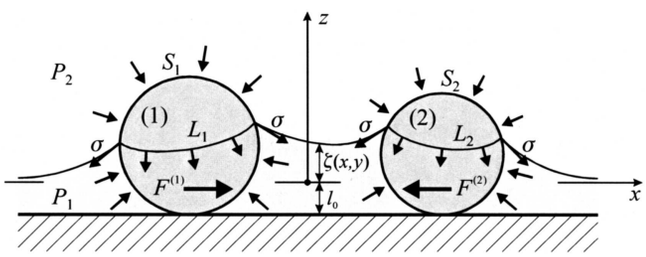

Fig. 16. Illustration of the origin of capillary force between two spheres partially immersed in a liquid film: the net horizontal force $\mathbf{F}^{(1)}$ exerted on particle 1 is a sum of the surface tension vector σ integrated along the contact line L_1 and of the pressure distribution integrated throughout the particle surface S_1 (the same for particle 2), see Eqs. (4.1)–(4.3).

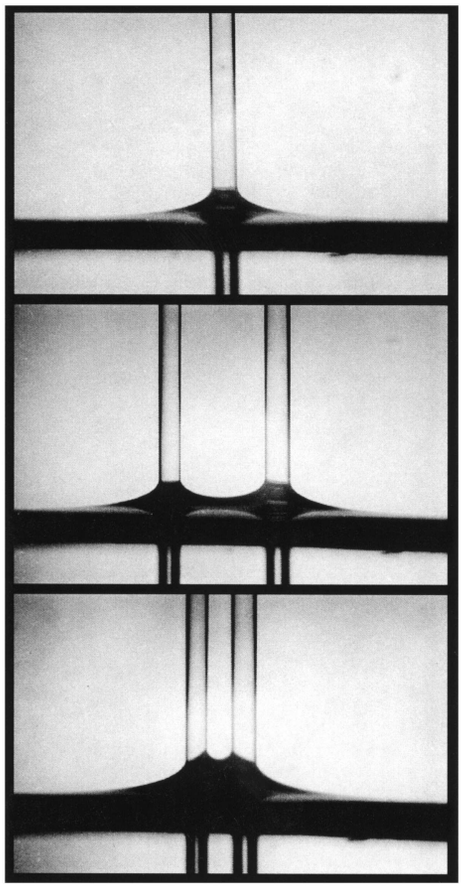

Fig. 17. Photographs, taken by Velev et al. [64], of two partially immersed vertical hydrophilic glass rods of radii $r_1 = 315$ μm and $r_2 = 370$ μm. Note that the inclination of the three-phase contact lines on the rods increases when the distance between them decreases.

horizontal (Fig. 17a); when two such rods approach each other inclination of the contact line appears (Fig. 17b) and grows with the decrease of the distance between the rods (Fig. 17c).

Imagine now that the upper part of the rods shown in Fig. 17 is hydrophobic, whereas the lower part is hydrophilic. In such a case the three-phase contact line can stick to the horizontal boundary between the hydrophobic and hydrophilic regions and the contact line will remain immobile and horizontal (no inclination!) when the two rods approach each other. Nevertheless, in such a case a lateral force of capillary attraction will also appear [21] because of the contact angle hysteresis: the meniscus slope varies along the circular contact line of each rod. The meniscus slope is the smallest in the zone between the two vertical cylinders (rods); then the

integration in Eq. (4.2) yields an attractive net force, see Kralchevsky and Nagayama [21] for more details.

It is worth noting that for small particles, $r_1,r_2 \ll q^{-1}$, the contribution of the pressure to the capillary force is negligible [19,20],

$$|\mathbf{F}^{(ip)}| \ll |\mathbf{F}^{(i\sigma)}| \quad \text{for } r_1,r_2 \ll q^{-1} \tag{4.4}$$

As established by Allain and Cloitre [49], the pressure contribution can prevail for $\zeta(r_i) \gg q^{-1}$ $(i = 1,2)$, i.e. for large Bond numbers; however, this is not the case with colloidal particles, for which Eq. (4.4) is applicable.

It is not obvious that the energy and force approaches, based on Eqs. (3.13)–(3.15) and Eqs. (4.1)–(4.3), respectively, are equivalent. Numerical coincidence of the results provided by these two approaches has been established in Kralchevsky et al. [19,20]. Analytical proof of the equivalence of the two approaches has been given in Kralchevsky and Nagayama [21] for the case of two vertical cylinders.

4.2. Asymptotic expression for the capillary force

As demonstrated in Fig. 16, the appearance of a small inclination of the contact line gives rise to the lateral capillary force. The mere superposition approximation is too rough to provide a quantitative estimate of this fine inclination. Indeed, the meniscus shape in superposition approximation does not satisfy the boundary condition for the constancy of the contact angle at the particle surface. A quantitative description can be obtained by solving the linearized Laplace equation, Eq. (3.6), in bipolar (bicylindrical) coordinates (τ, ω) in the plane xy, see e.g. Korn and Korn [60]

$$x = \frac{a\sinh\tau}{\cosh\tau - \cos\omega}, \quad y = \frac{a\sin\omega}{\cosh\tau - \cos\omega} \tag{4.5}$$

$$-\tau_1 \le \tau \le \tau_2, \quad -\pi \le \omega \le \pi \tag{4.6}$$

The elementary lengths along the τ- and σ-lines of the respective orthogonal curvilinear coordinate network are [60]

$$dl_\tau = \sqrt{g_{\tau\tau}}\,d\tau, \quad dl_\omega = \sqrt{g_{\omega\omega}}\,d\omega, \quad g_{\tau\tau} = g_{\omega\omega} = \frac{a^2}{(\cosh\tau - \cos\omega)^2} \tag{4.7}$$

where $g_{\tau\tau}$ and $g_{\omega\omega}$ are components of the metric tensor. In Fig. 18 the circumferences C_1 and C_2, of radii r_1 and r_2, represent the projections of the contact lines L_1 and L_2 on two interacting particles onto the plane xy (see e.g. Fig. 16). The x-axis is chosen to pass through the centers of the two circumferences. The coordinate origin is determined in such a way that the tangents OA_1 and OA_2 to have equal lengths, a, see Fig. 18; in fact this is the geometrical meaning of

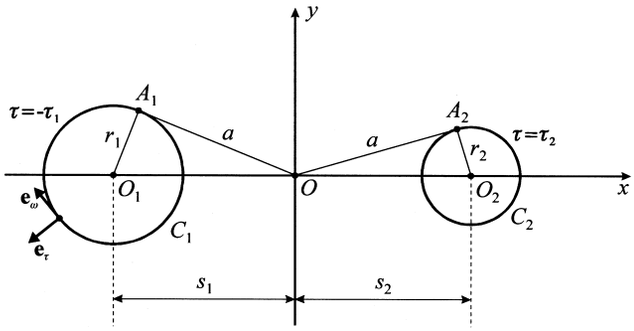

Fig. 18. Introduction of bipolar coordinates, in the plane xy, see Eq. (4.5): the x-axis passes through the centers O_1 and O_2 of the contact line projections C_1 and C_2; the coordinates origin O is located in such a way that the two tangents, OA_1 and OA_2, have equal length a.

parameter a in Eqs. (4.5) and (4.7). From the two rectangular triangles in Fig. 18 one obtains

$$s_i^2 - a^2 = r_i^2, \quad (i = 1,2). \tag{4.8}$$

The two circumferences in Fig. 18 correspond to fixed values of the parameter τ, as follows: $\tau = \tau_1$ and $\tau = \tau_2$, where τ_1 and τ_2 are related to the geometrical parameters as follows:

$$\cosh\tau_i = s_i/r_i, \quad \sinh\tau_i = a/r_i \quad (i = 1,2). \tag{4.9}$$

A substitution of Eq. (4.9) into Eq. (4.8) yields the known identity $\cosh^2\tau_I - \sinh^2\tau_i = 1$.

Let us consider the capillary force $\mathbf{F}^{(2)}$ exerted on particle 2. In view of Eqs. (4.1)–(4.4) one can write

$$\mathbf{F}^{(2)} \approx \mathbf{F}^{(2\sigma)} \approx \sigma \oint_{C_2} dl(\mathbf{U}_{\mathrm{II}} \cdot \mathbf{m}) \tag{4.10}$$

where approximation for small meniscus slope has been used to reduce the integration along the contact line L_2 to integration along its projection C_2. By means of geometrical considerations one can derive [19]

$$\mathbf{U}_{\mathrm{II}} \cdot \mathbf{m} = \mathbf{e}_\omega \frac{d\zeta}{dl} \sin\psi_2 + \mathbf{e}_\tau \cos\psi_2 \tag{4.11}$$

where ψ_2 is the meniscus slope angle at the contact line of particle 2, see e.g. Fig. 1; $\mathbf{e}_\omega$ and $\mathbf{e}_\tau$ are running unit vectors of the coordinate lines; in our case $\mathbf{e}_\omega$ is tangential to the contour C_2, whereas $\mathbf{e}_\tau$ is normal to it (Fig. 18). Now, let us

substitute Eq. (4.11) into Eq. (4.10); the result reads

$$\mathbf{F}^{(2)} \approx \sigma \sin\psi_2 \oint_{c_2} dl \frac{d\zeta}{dl} \mathbf{e}_\omega = \sigma \sin\psi_2 \int_{-\pi}^{\pi} d\omega \frac{d\zeta_2}{d\omega} \mathbf{e}_\omega \tag{4.12}$$

where $z = \zeta_2(\omega)$ describes the shape of the contact line on the surface of particle 2. In Eq. (4.12) we have used the assumption that $\psi_2 \approx$ const., which is rigorous for vertical cylinders, but is a good approximation also for small spherical particles; the integral of the term with $\mathbf{e}_\tau$ in Eq. (4.11) is equal to zero. Using the relationships between curvilinear and Cartesian coordinates one obtains [60]

$$\mathbf{e}_\omega = \frac{1}{\sqrt{g_{\omega\omega}}} \left(\mathbf{e}_x \frac{\partial x}{\partial \omega} + \mathbf{e}_y \frac{\partial y}{\partial \omega} \right) \tag{4.13}$$

where $\mathbf{e}_x$ and $\mathbf{e}_y$ are the unit vectors of the x- and y-axes. With the help of Eqs. (4.5)–(4.7) and (4.13) one can transform Eq. (4.12) to read

$$\mathbf{F}^{(2)} = \mathbf{e}_x F_x; \quad F_x \approx -\sigma \sin\psi_2 \int_{-\pi}^{\pi} d\omega \frac{\sinh\tau_2 \sin\omega}{\cosh\tau_2 - \cos\omega} \frac{d\zeta_2}{d\omega} \tag{4.14}$$

4.3. Shape of the contact line on the particle surface

Solving the Laplace equation in bipolar coordinates and using the method of the matched asymptotic expansions one can derive the following expression for the shape of the contact lines on the surfaces of the two interacting particles [22]:

$$\zeta_i(\omega) \approx h_{i\infty} + Q_j K_0 \left(\frac{2qa^2}{s_i - r_i \cos\omega} \right), \quad \left(\frac{r_i}{s_i} \right) \ll 1, \quad |\nabla_{\mathrm{II}} \zeta|^2 \ll 1 \tag{4.15}$$

($i \neq j$; $i, j = 1, 2$); here $h_{i\infty}$ is the elevation of the contact line for an isolated particle (cylinder); $h_{i\infty}$ is independent of ω. The term with K_0 in Eq. (4.15) expresses the perturbation in the shape of the contact line on the particle 'i', which is due to the presence of the particle 'j' at a finite distance $L = s_1 + s_2$. Next we expand Eq. (4.15) in series for $r_i/s_i \ll 1$ (then $s_1 \approx s_2 \approx a \approx L/2$):

$$\zeta_i(\omega) = h_{i\infty} + Q_j [K_0(qL) - 2r_i q K_1(qL) \cos\omega + \ldots] \quad (i = 1,2) \tag{4.16}$$

Differentiating Eq. (4.16) one obtains

$$\frac{d\zeta_i}{d\omega} \approx 2r_i Q_j q K_1(qL) \sin\omega \quad (i \neq j; i,j = 1,2) \tag{4.17}$$

Finally, we substitute Eq. (4.17) for $i = 2$ into Eq. (4.14), which along with Eq. (2.2) yields

$$F_x \approx -2\sigma Q_1 Q_2 q K_1(qL)\sinh\tau_2 \int_{-\pi}^{\pi} \frac{\sin^2\omega \; d\omega}{\cosh\tau_2 - \cos\omega} \approx -2\pi\sigma Q_1 Q_2 q K_1(qL) \tag{4.18}$$

At the last step we have used the identity [19]

$$\int_{-\pi}^{\pi} \frac{\sin^2\omega \; d\omega}{\cosh\tau_2 - \cos\omega} = 2\pi\exp(-\tau_2) \tag{4.19}$$

and the approximation

$$2\sinh\tau_2\exp(-\tau_2) \approx 1 \quad \text{for} \quad \tau_2 \geq 2 \quad (r_2/s_2 \ll 1) \tag{4.20}$$

see also Eq. (4.9).

As could be expected, the derived asymptotic expression for the lateral capillary force, Eq. (4.18), is identical to Eq. (2.1). Note that during the derivation of Eq. (4.18) it was not necessary to specify whether the capillary force is of flotation or immersion type, or whether we deal with a single interface or with a thin liquid film. We have used only the integral expression for the capillary force, Eq. (4.10), which is valid in all aforementioned cases, as well as Eq. (4.15) for the shape of the contact line. The latter equation accounts for the overlap of the interfacial deformations created by the two particles (cylinders) irrespective of the origin of the deformation: weight of the particle or capillary rise (wetting). Consequently, the above derivation of the expression for the capillary interaction by means of the force approach once again confirms the general conclusion that all kind of lateral capillary forces are due to the overlap of perturbations in the interfacial shape created by attached bodies.

Note that Eq. (4.18) is an approximate asymptotic formula, which is valid for comparatively long distances between the particles ($L \gg r_1, r_2$). More accurate analytical expressions for the capillary force, which are valid also for short interparticle separations, can be found in Kralchevsky et al. [14,18–22].

5. Capillary forces between particles at a spherical interface, film and membrane

5.1. Origin of the 'capillary charge' in the case of spherical interface

The spherical geometry provides some specific conditions, which differ from those with planar interfaces or plane–parallel thin films. For example, the capillary force between two diametrically opposed particles is zero irrespective of the range of the interaction determined by the characteristic capillary length q^{-1}. Moreover, in the case of spherical thin film the volume of the liquid layer is finite.

As already discussed, the particles attached to an interface (thin film, membrane) interact through the overlap of the perturbations in the interfacial shape created by them. Of course, this is true also when the non-disturbed interface is spherical; in this case any deviation from the spherical shape has to be considered as an interfacial perturbation, which gives rise to the particle 'capillary charge', see Section 2. As a rule, the effect of gravity is negligible in the case of spherical interfaces (otherwise the latter will be deformed), and consequently, it is not expected the particle weight to cause any significant interfacial deformation. Then a question arises: Which is the origin of the interfacial perturbations in this case?

Let us consider an example depicted in Fig. 19a: a solid spherical particle attached to the surface of a spherical emulsion drop of radius R_0. Such a configuration is typical for the Pickering emulsions which are stabilized by the adsorption of solid particles and have a considerable importance for the practice [81–83]. The depth of immersion of the particle into the drop phase, and the radius of the three-phase contact line, r_c, is determined by the value of the contact angle α (Fig. 19a). The pressure within the drop, P_{I}, is larger than the outside pressure P_{II} because of the curvature of the drop surface. The force pushing the particle outside the drop (along the z-axis) is

$$F_{\mathrm{out}} = \pi r_c^2 P_{\mathrm{I}}; \tag{5.1}$$

on the other hand, the force pushing the particle inside the drop is due to the outer pressure and the drop surface tension resolved along the z-axis (Fig. 19a):

$$F_{\mathrm{in}} = \pi r_c^2 P_{\mathrm{II}} + 2\pi r_c \sigma \sin\theta_c \tag{5.2}$$

Here θ_c is a central angle: $\sin\theta_c = r_c/R_0$. At equilibrium one must have $F_{\mathrm{in}} = F_{\mathrm{out}}$; then combining Eqs. (5.1) and (5.2) one obtains the Laplace equation $P_{\mathrm{I}} - P_{\mathrm{II}} = 2\sigma/R_0$ which is identically satisfied for a spherical interface. Thus we

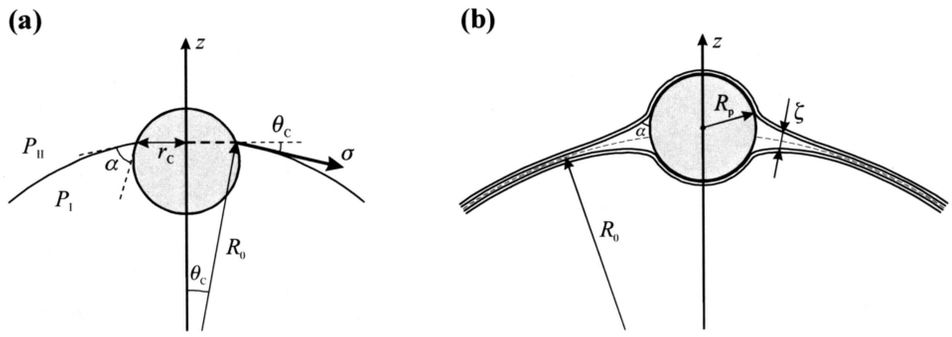

Fig. 19. (a) Spherical particle attached to the surface of an emulsion drop of radius R_0; α is the three phase contact angle; r_c is the contact line radius; P_{I} and P_{II} are the pressures inside and outside the drop. (b) Particle of radius R_p entrapped between the two lipid bilayers composing a spherical vesicle of radius R_0; ζ is the running thickness of the gap (filled with water) between the two detached bilayers.

arrive at the conclusion that the force balance $F_{in} = F_{out}$ is fulfilled for a spherical interface, *without* any deformation.

The same conclusion can be drawn on the basis of the Laplace equation. Indeed, the configuration of a spherical particle attached to an emulsion drop must have rotational symmetry. It is known [84] that for an axisymmetric surface intersecting the axis of revolution the Laplace equation, has a single solution: sphere (gravity deformation negligible). If a second particle is attached to the drop it can acquire the same configuration as that in Fig. 19a; only the radius of the spherical surface will slightly increase due to the volume of the drop phase displaced by the second particle. In other words the force balance $F_{in} = F_{out}$ is fulfilled for each separate particle and the drop surface remains spherical. However, if there is no deviation from the spherical shape, then lateral capillary force between the particles *cannot* appear. If aggregation of particles attached to such an emulsion drop is observed, it should be attributed to other kind of forces.

After the last 'negative' example, let us consider another illustrative example, in which both deformation and lateral capillary forces do appear. Pouligny and coworkers [85] have studied the sequence of phenomena which occur when a solid latex microsphere is brought in contact with an isolated giant spherical phospholipid vesicle. They observed a spontaneous attachment (adhesion) of latex particles to the vesicle, which is accompanied by complete or partial wetting (wrapping) of the particle by lipid bilayer(s). In fact, the membrane of such a vesicle can be composed of two or more lipid bilayers. As an example, in Fig. 19b we have depicted a possible configuration of a membrane consisting of two lipid bilayers; the particle is captured between the two bilayers. The experimental observations show that such two captured particles experience a long range attractive force [86]. There are experimental indications that in a vicinity of the particle the two lipid bilayers are detached (Fig. 19b) and a gap filled with water is formed between them [86]. The latter configuration resembles that depicted in Fig. 1f, and consequently, the observed long range attraction could be attributed to the capillary immersion force [86]. Similar configurations can appear also around particles, which are confined in the spherical film intervening between two attached emulsion droplets, or in the globular emulsion films. In these cases the interfacial deformations are caused by the confinement of the particles within the film.

Looking for an example in biology, we should note that the cytoskeleton of a living cell is a framework composed of interconnected microtubules and filaments, which resembles a 'tensegrity' architectural system composed of long struts joined with cables, see e.g. Ingber [87,88]. Moreover, inside the cell a gossamer network of contractile microfilaments pulls the cell's membrane toward the nucleus in the core [88]. In the points where the microfilaments are attached to the membrane, concave 'dimples' will be formed, see Fig. 20a. On the other hand, at the points where microtubules (the 'struts') touch the membrane, the latter will acquire a 'pimple'-like shape, see Fig. 20b. Being deformations in the cell membrane, these 'dimples' and 'pimples' will experience lateral capillary forces, both attractive and repulsive, which can be employed to create a more adequate mechanical model of

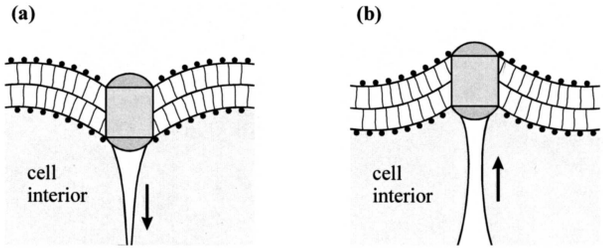

Fig. 20. Deformations in the membrane of a living cell due to (a) a microfilament pulling an inclusion inward and (b) a microtubule pushing an inclusion outward.

a living cell and, hopefully, to explain the regular 'geodesic forms' which appear in some biological structures [88].

Coming back to simpler systems, in which lateral capillary forces can be operative, we should mention the configuration of two small particles (Fig. 21), which are confined in a liquid film wetting a bigger spherical solid particle. The problem about the capillary forces experienced by two particles like those in Fig. 21 has been solved in Kralchevsky et al. [24]. Since the developed formalism is applicable also to the other systems mentioned above, in Section 5.2 we give an outline of this formalism.

5.2. Forces between particles entrapped in a spherical film

Let us consider the configuration depicted in Fig. 21: there is only one deformable surface and the two particles are identical. The non-disturbed spherical liquid film can have a stable equilibrium thickness h_0 only due to the action of some repulsive forces (positive disjoining pressure) between the two film surfaces. For that reason a *thin* film, i.e. a film for which the effect of the disjoining pressure Π is not negligible, has been considered in Kralchevsky et al. [24].

The radial coordinate of a point of the deformed film surface can be presented in the form

$$r = R_0 + \zeta(\theta,\varphi) \tag{5.3}$$

where θ and φ are standard polar and azimuthal angles on the reference sphere $r = R_0$ (Fig. 21) and $\zeta(\theta,\varphi)$ expresses the interfacial deformations due to the presence of the two particles. We assume small deformations, $|\zeta/R_0| \ll 1$ and $|\nabla_{\Pi}\zeta|^2 \ll 1$, where ∇_{Π} denotes surface gradient operator in the reference sphere. For such small deformations the Laplace equation for the film surface can be linearized [24]:

$$\nabla_{\Pi}^2\zeta - q^2\zeta = Q/R_0^2 \tag{5.4}$$

$$q^2 = -\frac{\Pi'}{\sigma_0} - \frac{2}{R_0^2} - \frac{2\Pi_0}{\sigma_0 R_0}, \quad Q = R_0\sin\theta_c\sin\psi_c, \tag{5.5}$$

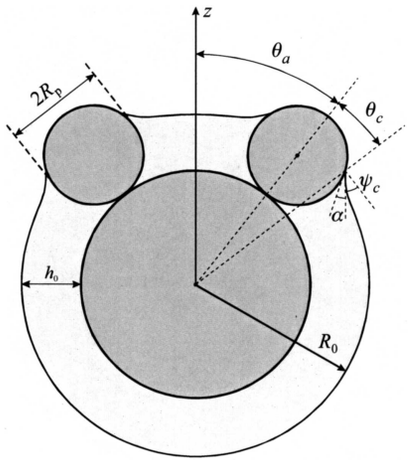

Fig. 21. Two particles of radius R_p confined in a liquid film around a larger spherical particle; θ_a and θ_c are angles characterizing the distance between the two particles and the position of the three-phase contact line on the particle surface; α and ψ_c are contact angle and meniscus slope angle; R_0 is the radius of the non-disturbed spherical fluid interface and h_0 is the thickness of the non-disturbed liquid film.

where q^{-1} is the characteristic capillary length, Q is the capillary charge, σ_0 and Π_0 are the surface tension and disjoining pressure of the non-disturbed spherical film of thickness h_0.

To conveniently integrate Eq. (5.4) special bipolar coordinates on a sphere have been introduced. The connection between the Cartesian coordinates (x,y,z) and the spherical bipolar coordinates (r,ω,τ) are [24]:

$$x = \frac{r\sqrt{\lambda^2 - 1}\sinh\tau}{\lambda\cosh\tau - \cos\omega}, \quad y = \frac{r\sqrt{\lambda^2 - 1}\sin\omega}{\lambda\cosh\tau - \cos\omega}, \quad z = \frac{r(\cosh\tau - \lambda\cos\omega)}{\lambda\cosh\tau - \cos\omega}. \tag{5.6}$$

The surfaces $r = \text{const.}$ are spheres; the lines $\omega = \text{const.}$ (on each sphere $r = \text{const.}$) are circumferences which are counterparts of the meridians; the lines $\tau = \text{const.}$ are circumferences-counterparts of the parallels of latitude, see Fig. 22a. In each point on the sphere the τ-line is orthogonal to the respective ω-line. In our case $r = R_0$ and $\lambda = \cos\theta_c/\cos\theta_a$, see Fig. 21 for the notation. The contact lines on the two particles correspond to $\tau = \pm\tau_c$, where [24]:

$$\tau_c \equiv \operatorname{arctanh}\left[(\cos^2\theta_c - \cos^2\theta_a)^{1/2}/\sin\theta_a\right] \quad (\theta_c < \theta_a \leq \pi/2) \tag{5.7}$$

Thus the domain of integration acquires the simple form of a rectangle, see Fig. 22b:

$$-\pi \leq \omega \leq +\pi, \quad -\tau_c \leq \tau \leq +\tau_c. \tag{5.8}$$

In spherical bipolar coordinates the linearized Laplace equation Eq. (5.4) has the form [24]

$$(\lambda\cosh\tau - \cos\omega)^2\left(\frac{\partial^2\tilde{\zeta}}{\partial\omega^2} + \frac{\partial^2\tilde{\zeta}}{\partial\tau^2}\right) = (qR_0)^2(\lambda^2 - 1)\tilde{\zeta}(\omega,\tau) \tag{5.9}$$

where $\tilde{\zeta} \equiv \zeta/R_0 + Q/(q^2R_0^3)$. In Ref. [24] Eq. (5.9) has been solved numerically using boundary conditions for (i) fixed contact angle and (ii) fixed contact line. Then the lateral capillary force, F, exerted on each particle (Fig. 21) has been calculated by means of integral expressions stemming from the force approach, see Section 4 above. For example, the expression for F corresponding to fixed contact line reads [24]:

$$F = -\sigma_0 R_0\int_0^{\pi} d\omega(\lambda\cosh\tau_c\cos\omega - 1)\left[\frac{1}{(\lambda^2 - 1)^{1/2}}\left(\frac{\partial\tilde{\zeta}}{\partial\tau}\right)^2 + \frac{2\sin\theta_c}{\lambda\cosh\tau_c - \cos\omega}\frac{\partial\tilde{\zeta}}{\partial\tau}\right]_{\tau=\tau_c} \tag{5.10}$$

Next, from the calculated values of F one can determine the capillary interaction energy:

$$\Delta W(L) = \int_L^{\pi R_0} F(L)dL \tag{5.11}$$

where $L = 2\theta_a R_0$ is the length of the (shortest) arc on the reference sphere connecting the centers of the two particles (Fig. 21). The additive constant in the energy is determined in such a way, that $\Delta W = 0$ for two diametrically opposed particles, i.e. for $L = \pi R_0$.

The calculated in Kralchevsky et al. [24] dimensionless interaction energy, $\Delta\tilde{W} = \Delta W/(\sigma_0 R_0^2)$, is plotted against the dimensionless distance, $\tilde{L} = L/(\pi R_0)$, in Figs. 23 and 24 ($2\theta_c/\pi \leq \tilde{L} \leq 1$). Note that $\Delta\tilde{W}$ is independent of σ_0 and R_0. The right-hand side scale in Figs. 23 and 24 shows the values of $\Delta W/kT$ (k is Boltzmann constant, T is temperature) for typical parameters values: $R_0 = 1$ μm, $\sigma_0 = 30$ mN/m, $T = 298$ K. At a given R_0, the size of the particles is determined by the angle θ_c, which for the curves in Figs. 23 and 24 takes values 1°, 2° and 3°, i.e. the particles are small, $r_c \ll R_0$. One sees in Figs. 23 and 24 that the interaction energy can be of the order of (10–100)kT. Physically $\Delta W/kT \gg 1$ means that the capillary attraction prevails over the thermal motion and can bring about particle aggregation and ordering in the spherical film. Such a situation is typical for the lateral capillary force of immersion type, see Section 2 above.

Note that the parameters values in Figs. 23 and 24 are chosen in such a way, that the shape of the fluid interfaces to be identical in the state of zero energy, i.e. for two diametrically opposed particles. This provides a basis for quantitative compar-

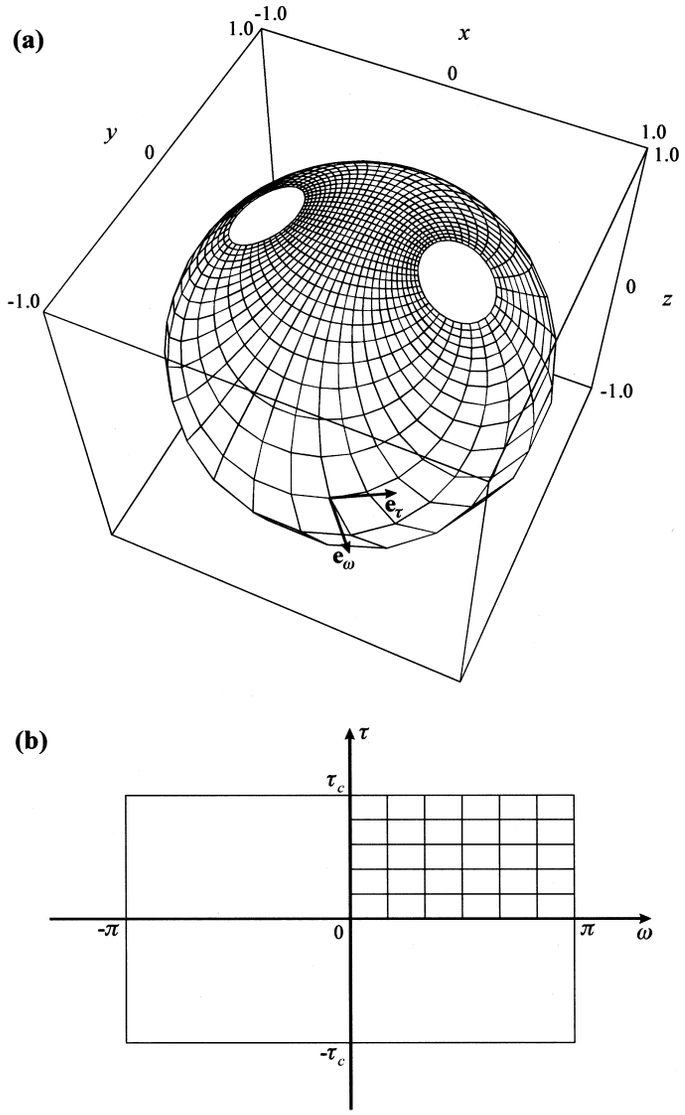

Fig. 22. (a) Bipolar coordinate lines on the unit sphere: the lines τ = const. are analogous to the parallels, while the lines ω = const. connecting the 'poles' resemble meridians, cf. Eq. (5.6). (b) The parameterization of the reference sphere, $r = R_0$ in Fig. 21, by means of spherical bipolar coordinates reduces the integration domain to a rectangle.

ison of the plots of ΔW vs. $\tilde{L}$ in Figs. 23 and 24, calculated by using the two alternative boundary conditions. The curves in Fig. 23 are calculated assuming fixed contact *angle*; one sees that the interaction energy ΔW is always negative, i.e. corresponds to attraction. On the other hand, the curves in Fig. 24 are calculated

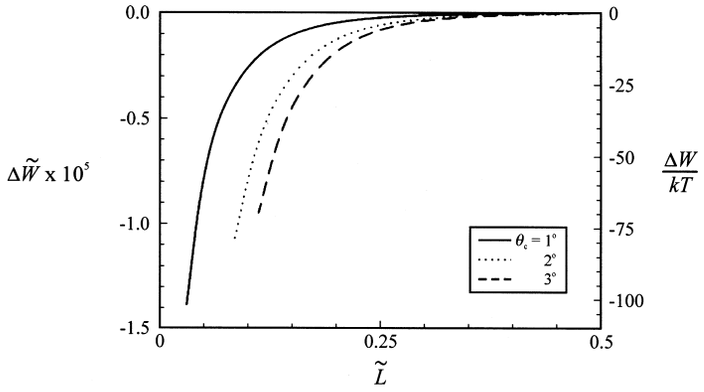

Fig. 23. Calculated in Kralchevsky et al. [24] dimensionless energy, $\Delta\tilde{W} = \Delta W/(\sigma_0 R_0^2)$, of capillary interaction between two particle plotted vs. the dimensionless interparticle separation $\tilde{L} = L/(\pi/R_0)$ for the case of fixed contact angle; the different curves correspond to different values of θ_c denoted on the figure; the other parameters values are $\psi_c = 5°$ and $qR_0 = 5$. The right-hand-side scale of $\Delta W/kT$ shows the interaction energy in the special case of $R_0 = 1$ μm, $\sigma_0 = 30$ mN/m and $T = 298$ K.

assuming fixed contact *line*. In the latter case the interaction energy changes its sign at comparatively large interparticle distances: attractive at short distances becomes repulsive at large separations.

The fact that that the interaction energy can change sign in the case of fixed contact *line*, but the energy is always negative in the case of fixed contact *angle*, is discussed in Kralchevsky et al. [24]. It is concluded that the non-monotonic behavior of the capillary interaction energy (Fig. 24) is a non-trivial effect stemming

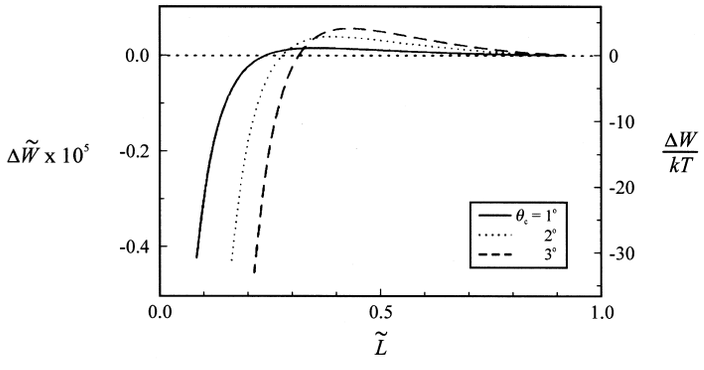

Fig. 24. Calculated in Kralchevsky et al. [24] dimensionless energy, $\Delta\tilde{W} = \Delta W/(\sigma_0 R_2^0)$, of capillary interaction between two particles plotted vs. the dimensionless interparticle separation $\tilde{L} = L/(\pi/R_0)$ for the case of fixed contact line and $qR_0 = 5$; the different curves correspond to different values of θ_c denoted on the Fig. 24; for each curve h_c/R_0 is fixed and equal to the respective values of h_∞/R_0 (0.00389, 0.00585 and 0.00719) for the curves in Fig. 23. The right-hand-side scale of $\Delta W/kT$ is as in Fig. 23.

from the *spherical* geometry of the film coupled with the boundary condition of fixed contact line; such an effect is difficult to anticipate by physical insight. Note that in the case of *planar* geometry the capillary force between identical particles is always monotonic attraction.

6. Lateral capillary forces between inclusions in lipid membranes

6.1. Perturbation of the lipid molecules due to inclusions in the membrane

The experiment shows that some integral (transmembrane) proteins can form two-dimensional ordered aggregates in native membranes [89–94]. To explain the driving force of this process a theory of lipid-mediated interactions between the membrane proteins has been developed in several works [95–98]. This theoretical approach is based on experimental findings that proteins incorporated in membranes perturb the neighboring lipid molecules [99–101], and especially affect the fluidity of their hydrocarbon chains. More recent experiments performed by means of ESR and NMR methods [102–104] demonstrated that the degree of ordering and fluidity of the hydrocarbon chains of lipid molecules bound to membrane proteins is not very different from those of free molecules, in contract with the initial hypotheses [95,96].

Other idea about the origin of the membrane-mediated interactions between inclusions stems from the experiments by Chen and Hubbell [105], who have observed aggregation of the transmembrane protein rhodopsin in cases in which there has been a *mismatch* between the width of the hydrophobic belt of the protein and the thickness of the hydrophobic interior of the lipid bilayer, see Fig. 3. One can conclude that the perturbation of the bilayer thickness in a vicinity of an incorporated protein may give rise to protein–protein attraction. This effect was studied both experimentally [106–110] and theoretically [111–114,25,46]. Lewis and Engelman [107] showed that bacteriorhodopsin forms aggregates in vesicles (prepared from lipids of different chain length) only when the mismatch is greater than 1 nm for thinner bilayers (Fig. 3a) and 0.4 nm for thicker bilayers (Fig. 3b). Likewise, protein aggregation at considerable hydrophobic mismatch was detected with other natural proteins [106,108,109] and synthesized polypeptides [108].

In Kralchevsky et al. [25] we proposed a theoretical approach to the membrane mediate interaction between inclusions, which is based on an extension of the theory of the lateral capillary forces described above. The extension is needed because the mechanical properties of a lipid bilayer differ from the properties of a common thin liquid film. For that reason, prior to the calculation of the capillary force, an appropriate ‘sandwich’ model of the lipid membrane has been developed, which is described briefly below.

6.2. Sandwich model of a lipid bilayer

A lipid bilayer drawn to scale is shown in Fig. 25. One can distinguish a

hydrophobic hydrocarbon chain region sandwiched between two hydrophilic regions of the lipid polar headgroups. It is generally accepted that a lipid bilayer behaves as a *two-dimensionalviscous fluid* at body temperature. This two-dimensional fluidity is manifested when inclusions are moving throughout the membrane [115]. On the other hand, the bilayer exhibits *elastic* properties in processes of dilatation or bending, both of them being accompanied by extension or compression of the hydrocarbon chains of the lipids. In other words, a bilayer can exhibit different rheological behavior (fluid, elastic or hybrid) depending on the mode of deformation. This is not surprising, because a bilayer is neither a three-dimensional, nor a two-dimensional continuum and the hydrocarbon region is neither an isotropic liquid, nor a solid. A natural approach to the mechanics of such a complex body is to use different constitutive relations (connecting stress and strain) for the different independent modes of deformation. The displacement vector **u** can be expressed as a sum of components due to the independent modes [25]:

$$\mathbf{u} = \mathbf{u}_{\text{stretching}} + \mathbf{u}_{\text{bending}} + \mathbf{u}_{\text{squeezing}} \tag{6.1}$$

In the case of bending or uniform stretching the bilayer is modeled as an incompressible elastic body sandwiched between two Gibbs dividing surfaces (modeling the two headgroup regions, see Fig. 25). Then the following expressions for the bilayer elastic parameters have been obtained [25]:

$$K_s = 2\sigma + 2E_G + 3\Pi h + 3\lambda h \qquad \text{(stretching elastic modulus)} \tag{6.2}$$

$$k_t = 2k_c - (\tfrac{3}{4}B_0 + \tfrac{1}{2}B')h + \tfrac{1}{2}E_G h^2 + \tfrac{1}{3}\lambda h^3 \quad \text{(bending elastic modulus)} \tag{6.3}$$

$$\bar{k}_t = 2\bar{k}_c + \tfrac{1}{2}B_0 h - \tfrac{1}{6}\lambda h^3 \quad \text{(torsion elastic modulus)} \tag{6.4}$$

Here K_s is the stretching elastic modulus of the bilayer as a whole; σ and E_G are the interfacial tension and the Gibbs elasticity of a lipid *monolayer* on a hydrocarbon–water interface at the same temperature, composition of the aqueous phase and area per molecule as for the bilayer; Π is disjoining pressure which is expected to originate mostly from the van der Waals forces [25]; h is the thickness of the hydrocarbon interior of the lipid bilayer, which is modeled as an incompressible elastic plate having shear elasticity λ; $B = B_0 + B'\alpha + \ldots$ is the series expansion of the bending moment of the bilayer surface for small values of the relative dilatation $\alpha = \Delta A/A$ of the interfacial area A; k_c and $\bar{k}_c$ are the bending and torsion elastic moduli of the bilayer surfaces (to be distinguished from k_t and $\bar{k}_t$, which characterize the bilayer as a whole).

The deformation of a bilayer of (non-disturbed) thickness h around a cylindrical inclusion (say a transmembrane protein) having a hydrophobic belt of width l_0 consists of a variation of the bilayer thickness at planar midplane (Fig. 26). Such a mode of deformation corresponds to the *squeezing* (peristaltic) mode observed with thin liquid films [116]. The extension of the lipid hydrocarbon chains along the z-axis is greater for molecules situated closer to the inclusion (Fig. 26). The region

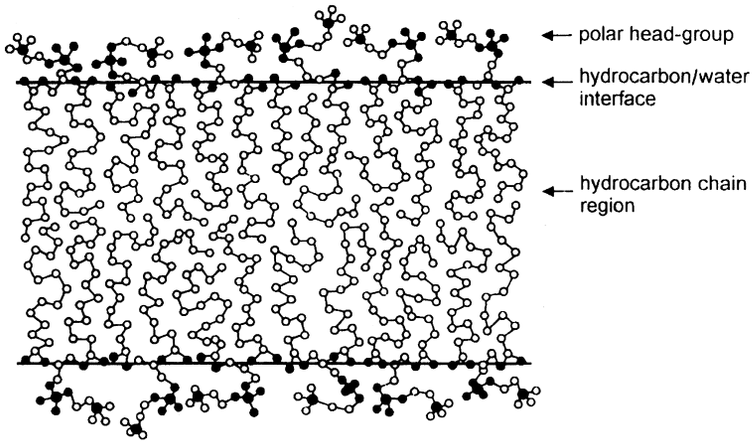

Fig. 25. A lipid (lecithin) bilayer drawn to scale (after Israelachvili [117]).

of the hydrocarbon chains of a separate lipid molecule (one of the many small rectangles depicted in Fig. 26) exhibit an elastic response to extension–compression; therefore each of them can be modeled as an incompressible elastic body. On the other hand, lateral slip between molecules (neighboring rectangles in Fig. 26) should not be accompanied with any elastic effects because of the two-dimensional fluidity of the bilayer. Both these requirements are accounted for in the following mechanical constitutive relation for the stress tensor τ_{ij}[25]:

$$\tau_{zz} = 2\lambda \frac{\partial u_z}{\partial z}; \quad \tau_{ij} = -p\delta_{ij}, \quad (i,j) \neq (z,z) \quad i,j = x,y,z \tag{6.5}$$

Here δ_{ij} is the Kroneker symbol, p has the meaning of pressure characterizing the bilayer as a two-dimensional fluid; u_z is the z-component of the displacement vector **u**; the coordinate system is depicted in Fig. 26. The mechanical conditions for hydrostatic equilibrium and incompressibility yield:

$$\frac{\partial \tau_{ij}}{\partial x_i} = 0, \quad j = 1,2,3; \quad \nabla \cdot \mathbf{u} = 0 \quad (x_1 = x,\ x_2 = y,\ x_3 = z), \tag{6.6}$$

where τ_{ij} is to be substituted from Eq. (6.5). Thus the mechanical problem is formulated: Eq. (6.6) represent a set of four equations for determining the four unknown functions u_x, u_y, u_z and p. Considerations of symmetry imply that u_z must be an odd function of z which is to satisfy the boundary condition

$$u_z = \zeta(x,y) \quad \text{for } z = h/2, \tag{6.7}$$

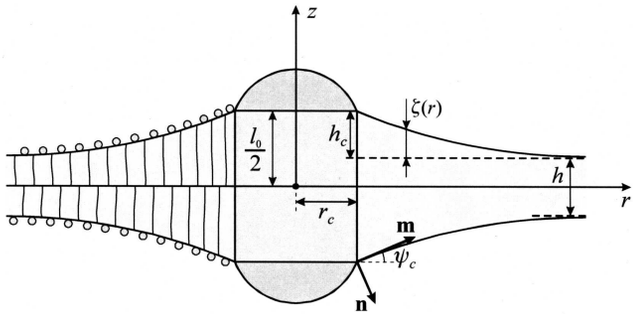

Fig. 26. Sketch of the deformation around a cylindrical inclusion (membrane protein) of radius r_c and width of the hydrophobic belt l_0; h is the thickness of the non-disturbed bilayer and h_c is the mismatch between the hydrophobic regions of the inclusion and the bilayer (after Kralchevsky et al. [25]).

where $z = \zeta(x,y)$ describes the shape of the upper bilayer surface. In Kralchevsky et al. [25] it is proven that $\zeta(x,y)$ can be found as a solution of the equation

$$\nabla_{\mathrm{II}}^2\zeta = q^2\zeta \tag{6.8}$$

which has the same form as Eq. (3.6), but the capillary length q^{-1} is defined in a different way [25]:

$$q^2 = \frac{1}{2k_c}\left\{\tilde{\sigma}_0^2 - \left[\tilde{\sigma}_0^2 - 8k_c(2\lambda/h - \Pi')\right]^{1/2}\right\} \approx \frac{4\lambda}{h\tilde{\sigma}_0} \tag{6.9}$$

Here $\tilde{\sigma}_0 \equiv \sigma_0 + B'/h$, with σ_0 being the surface tension of the non-disturbed planar bilayer far from the inclusion. The solution of Eq. (6.8) for a *single* cylindrical inclusion along with the boundary condition for constant elevation, $\zeta = h_c$, at the contact line (Fig. 26), yields

$$\zeta = \frac{h_c}{\mathrm{K}_0(qr_c)}\mathrm{K}_0(qr) \quad (r \geq r_c) \tag{6.10}$$

where, as usual, r is the radial coordinate and r_c is the radius of the inclusion. For a *couple* of inclusions one can solve Eq. (6.8) in bipolar coordinates, which are introduced as explained in Section 4.2 above, see Kralchevsky et al. [25] for details.

6.3. Capillary interaction between inclusions

The force approach (Section 4.1) can be applied to calculate the lateral capillary force, **F**, between a couple of cylindrical inclusions, like those depicted in Figs. 3 and 26:

$$\mathbf{F} = 2\mathbf{U}_{\mathrm{II}} \cdot \oint_c dl(\mathbf{m} \cdot \underline{\sigma}) \tag{6.11}$$

Here C denotes the contact line; the multiplier 2 accounts for the presence of two identical contact lines (upper and lower) on each inclusion; Eq. (6.11) looks like Eq. (4.2) with the only difference that for a membrane the surface tension is a tensor, $\underline{\sigma}$, rather than a scalar [25]:

$$\underline{\sigma} = \mathbf{U}_s\sigma + \mathbf{a}_\mu \mathbf{n}\sigma^{\mu(n)} \tag{6.12}$$

Here σ is the scalar surface tension, $\mathbf{U}_s$ is a unit tensor in the film surface, $\mathbf{a}_\mu$ ($\mu = 1,2$) are the vectors of a local basis in the bilayer surface, $\mathbf{n}$ is the running unit normal to this surface (Fig. 26) and the transversal components $\sigma^{\mu(n)}$ are related to the divergence of the tensor of the surface moments, $M^{\mu\nu}$[25]:

$$\sigma^{\mu(n)} = -M^{\mu\upsilon}_{,\upsilon} = -(k_c q^2 - B'/h)\zeta_{,\mu} \tag{6.13}$$

Combining Eqs. (6.11)–(6.13) one can present the lateral capillary force as a sum of contributions, $\mathbf{F}^{(\sigma)}$ and $\mathbf{F}^{(B)}$, due to the surface tension and the interfacial bending moment, respectively [25]:

$$\mathbf{F} = \mathbf{F}^{(\sigma)} + \mathbf{F}^{(B)} \tag{6.14}$$

$$\mathbf{F}^{(\sigma)} = 2\oint_c dl(\mathbf{U}_{\mathrm{II}} \cdot \mathbf{m})\sigma \tag{6.15}$$

$$\mathbf{F}^{(B)} = 2(k_c q^2 - B'/h)\oint_c dl(\mathbf{m} \cdot \nabla_s\zeta)(\mathbf{U}_{\mathrm{II}} \cdot \mathbf{n}) \tag{6.16}$$

where ∇_s is a gradient operator in the curved surface $\zeta(x,y)$. The latter equations show that the interfacial bending moment can also give a contribution to the lateral capillary force: this conclusion has a general validity, i.e. it holds for any interface, not only for lipid membranes. However, it is to be expected, that $\mathbf{F}^{(B)}$ can be comparable by magnitude with $\mathbf{F}^{(\sigma)}$ only for interfaces of low tension, such as microemulsions, some emulsions and biomembranes (otherwise one could expect that $\mathbf{F}^{(\sigma)} \gg \mathbf{F}^{(B)}$).

In the case of two identical cylindrical inclusions in a lipid membrane (like those in Fig. 3) one can introduce bipolar coordinates (see Section 4.2) in Eqs. (6.15) and (6.16) to derive an expression for the non-zero x-component of the lateral capillary force $\mathbf{F}$ [25]:

$$F_x = -\frac{2}{a}(\tilde{\sigma}_0 - k_c q^2)\int_0^\pi d\omega(\cosh\tau_c\cos\omega - 1)\left(\frac{\partial\zeta}{\partial\tau}\right)^2_{\tau=\tau_c} \tag{6.17}$$

Here a and τ_c are defined by Eqs. (4.8) and (4.9), where for two identical inclusions of radius r_c we have set $s_1 = s_2 = L/2$, $r_1 = r_2 = r_c$, $\tau_1 = \tau_2 = \tau_c$, with L being

the distance between the axes of the two cylindrical inclusions. Note that the force F_x can be attractive or repulsive depending on whether $\tilde{\sigma}_0 > k_c q^2$ or $\tilde{\sigma}_0 < k_c q^2$. The respective interaction energy can be obtained by integration:

$$\Delta\Omega(L) = \int_L^\infty F_x(L)dL \tag{6.18}$$

In Kralchevsky et al. [25] an asymptotic formula for $\Delta\Omega(L)$ has been derived, which reads:

$$\Delta\Omega(L) = 4\pi(\tilde{\sigma}_0 - k_c q^2)qr_c h_c^2\left[\frac{K_1(qr_c) - \frac{1}{2}qr_c K_0(qL)}{K_0(qr_c) + K_0(qL)} - \frac{K_1(qr_c)}{K_0(qr_c)}\right] \tag{6.19}$$

The numerical test of Eq. (6.19) shows that it gives $\Delta\Omega(L)$ with a good accuracy.

To examine the predictions of Eq. (6.19) parameters of the bacteriorhodopsin molecule have been used: $r_c = 1.5$ nm and $l_0 = 3.0$ nm, see Fig. 26 for the notation. The following values of the bilayer mechanical parameters have been used: $\lambda = 2 \times 10^6$ N/m^2, $\sigma_0 = 35$ mN/m and $B' = -3.2 \times 10^{-11}$ N; with $h = 3$ nm one calculates $B'/h \approx -11$ mN/m, $\tilde{\sigma}_0 \equiv \sigma_0 + B'/h \approx 24$ mN/m and $q^{-1} \approx 3$ nm; in this case the term $k_c q^2 \approx 0.4$ mN/m is negligible compared to $\tilde{\sigma}_0$, see Kralchevsky et al. [25]. The mismatch between the height of the cylindrical inclusion, l_0, and the thickness of the non-disturbed layer, h, can be characterized by the quantity $h_c = (l_0 - h)/2$, see Fig. 26. In the experiments of Lewis and Engelman [107] l_0 was fixed and h was varied by using various lipids. The same experimental values of h have been used in our calculations: they are denoted on the respective curves in Fig. 27a,b, all of them corresponding to the same value of l_0 (to the same protein). The calculated curves of $\Delta\Omega/kT$ vs. $L/(2r_c)$ for $h_c > 0$ are shown in Fig. 27a, whereas those for $h_c < 0$ are shown in Fig. 27b. In general, one sees that the strength of the lateral capillary attraction increases with the increase of the mismatch magnitude $|h_c|$. Comparing the curves with the same magnitude, but opposite signs of h_c ($h_c = 0.2$ for the curve with $h = 2.6$ nm in Fig. 27a, while $h_c = -0.2$ for the curve with $h = 3.4$ nm in Fig. 27b), one can conclude, that has larger magnitude and longer range in the case of $h_c < 0$ (bilayer thicker than the inclusion). This result is consonant with the experimental observations of Lewis and Engelman [107].

We compare $\Delta\Omega$ with the energy of the thermal motion kT, for 25°C. One can see in Fig. 27 that for both $h_c > 0$ and $h_c < 0$ the energy of capillary attraction is larger than the thermal energy, except for $h = 2.6$ and 3.4 nm for which the mismatch is rather small. In the two limiting cases of large mismatch, $h = 1.55$ and 3.75 nm, the interaction energy is large enough at close contact, $\Delta\Omega = 5$–$10\ kT$, to cause aggregation of the membrane proteins. It is worth noting that only in the latter two limiting cases have Lewis and Engelman [107] observed protein aggregation. A more detailed discussion of the comparison between theory and experiment can be found in Kralchevsky et al. [25,48].

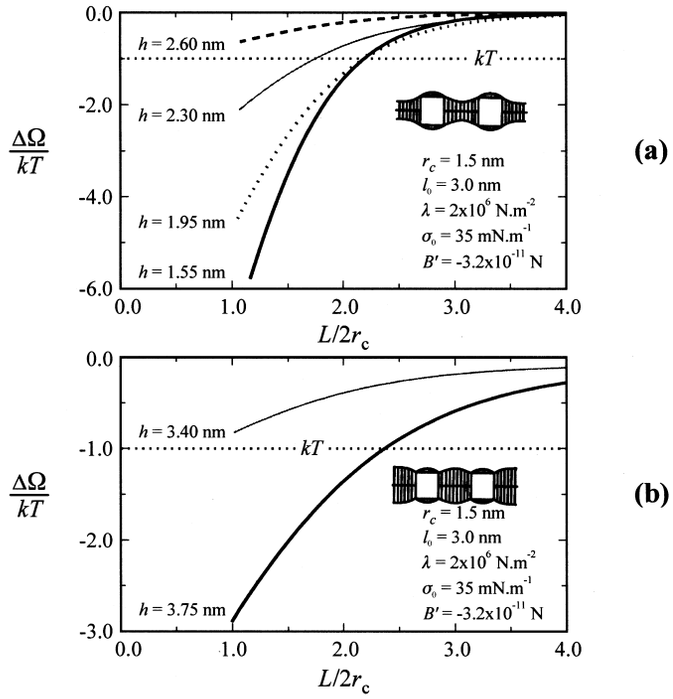

Fig. 27. Calculated in Kralchevsky et al. [25] interaction energy between two inclusions, $\Delta\Omega$, scaled by kT, vs. the separation L, scaled by r_c; the mechanical parameters of bilayer are $\lambda = 2 \times 10^6$ N/m^2, $\sigma_0 = 35$ mN/m and $B' = -3.2 \times 10^{-11}$ N; the geometrical parameters of bacteriorhodopsin molecule taken from Henderson [90] are $r_c = 1.5$ nm, $l_0 = 3.0$ nm and the values of h corresponds to the experiments in Lewis and Engelman [107]. (a) Thinner bilayer, $h - l_0 < 0$; (b) thicker bilayer, $h - l_0 > 0$.

7. Summary and conclusion

A general conclusion is that lateral capillary forces appear when the attachment of particles (or other bodies) to a fluid phase boundary is accompanied with perturbations in the interfacial shape; the capillary interaction itself is due to the overlap of such perturbations. The latter can appear around floating particles (Fig. 1a), around particles confined in a liquid film (Fig. 1b and f), between inclusions in lipid membranes (Fig. 3), between two vertical cylinders (Figs. 4 and 17), etc. In the case of floating particles the deformations in the meniscus shape are due to the particle weight. The 'flotation' capillary forces appearing in the latter case decrease with the sixth power of the particle size and become immaterial for particles smaller than approximately 10 μm. In all other cases the interfacial deformations are due to the surface wetting properties of particles or bodies, which are partially immersed in the two neighboring phases; the resulting 'immersion' capillary forces can be large enough (Fig. 2) to cause two-dimensional aggregation and ordering of small colloidal particles, which has been observed in many experiments.

The asymptotic law of the capillary interaction resembles the Newton law of gravity, or Coulomb's law in electrostatics, Eq. (2.3). The latter analogy enables one to introduce capillary charges of the attached particles, which can be both positive and negative. This analogy can be further extended to the capillary interaction between particle and wall, which resembles the image force in electrostatics, see Fig. 8. If a particle is moving bound to an interface under the action of a capillary force, one can determine the surface drag coefficient and the surface shear viscosity supposedly the magnitude of the capillary force is known (Figs. 9, 11 and 12).

There are two equivalent theoretical approaches to the lateral capillary interactions: energy and force approaches. Both of them require the Laplace equation of capillarity to be solved and the meniscus profile around the particles to be determined. The energy approach accounts for contributions due to the increase of the meniscus area, gravitational energy and/or energy of wetting, see Eq. (3.13). The second approach is based on calculating the net force exerted on the particle which can originate from the hydrostatic pressure, interfacial tension and bending moment, see Eqs. (4.1)–(4.3) and Eqs. (6.14)–(6.16). In the case of small overlap of the interfacial perturbations, created by two interacting bodies, the superposition approximation can be combined with the energy approach to derive an asymptotic formula for both flotation and immersion interaction, see Sections 3.2 and 3.3. This formula has been found to agree well with the experiment (Figs. 5 and 7). The force approach provides an unified derivation of the same formula (Section 4.2).

Capillary interactions between particles bound to spherical interfaces are also considered (Section 5). Due to the spherical geometry and restricted area the capillary forces in the latter case exhibit some differences from those in the case of planar interface. In particular, it turns out that the capillary force between identical particles can have a non-monotonic behavior (repulsion at long distances and attraction at short distances) unlike the respective force at flat interfaces, which is always attractive.

Finally, a similar approach can be applied to quantify the forces between inclusions (transmembrane proteins) in lipid membranes (Section 6). Such inclusions also give rise to deformations in the lipid membranes, which can be described theoretically in the framework of a mechanical model of the lipid bilayer (the 'sandwich' model), which accounts for the 'hybrid' rheology of a lipid bilayer (neither elastic body nor fluid), see Section 6.2. Lateral capillary forces can appear also between concave and/or convex formations ('dimples' and 'pimples') in the membrane of a living cell, which are due to mechanical stresses exerted by microfilaments and microtubules belonging to the cytoskeleton (Fig. 20).

In conclusion, the lateral capillary forces can appear in a variety of systems with characteristic particle size from 1 cm down to 1 nm; in all cases the capillary interaction has a similar origin (overlap of interfacial deformations) and is subject to a unified theoretical treatment.

Acknowledgements

The major part of this study was supported by the Research and Development Corporation of Japan (JRDC) under the Nagayama Protein Array Project of the program 'Exploratory Research for Advanced Technology'. The authors are indebted to Prof. I. B. Ivanov for the valuable suggestions and discussions, and to the team members Dr. N. D. Denkov, Dr. C. D. Dushkin, Dr. O. D. Velev and Dr. V. N. Paunov, who devoted much time and creative power to this study. Special gratitude is expressed to Mr Radostin Danev, who drew or adapted the figures in this article.

References

[1] D.F. Gerson, J.E. Zaijc, M.D. Ouchi, in: M. Tomlinson (Ed.), Chemistry for energy, ACS symposium series, 90, American Chemical Society, Washington DC, 1979, p. 66.
[2] J.D. Henry, M.E. Prudich, K.R. Vaidyanathan, Sep. Purif. Methods 8 (1979) 81.
[3] M.M. Nicolson, Proc. Cambridge Philos. Soc. 45 (1949) 288.
[4] K. Hinsch, J. Colloid Interface Sci. 92 (1983) 243.
[5] C. Allain, B Jouhier, J. Phys. Lett. 44 (1983) 421.
[6] C. Allain, M. Cloitre, in: R. Jullien et al. (Ed.), Springer proceedings in physics, 32, Springer Verlag, Berlin, 1988, p. 146.
[7] B.V. Derjaguin, V.M. Starov, Colloid J. USSR Engl. Trans. 39 (1977) 383.
[8] H. Yoshimura, S. Endo, M. Matsumoto, K. Nagayama, Y. Kagawa, J. Biochem. 106 (1989) 958.
[9] H. Yoshimura, M. Matsumoto, S. Endo, K. Nagayama, Ultramicroscopy 32 (1990) 265.
[10] L. Haggerty, B.A. Watson, M.A. Barteau, A.M. Lenhoff, J. Vac. Sci. Technol. B9 (1991) 1219.
[11] N.D. Denkov, O.D. Velev, P.A. Kralchevsky, I.B. Ivanov, H. Yoshimura, K. Nagayama, Langmuir 8 (1992) 3183.
[12] N.D. Denkov, O.D. Velev, P.A. Kralchevsky, I.B. Ivanov, H. Yoshimura, K. Nagayama, Nature (London) 361 (1993) 26.
[13] C.D. Dushkin, K. Nagayama, T. Miwa, P.A. Kralchevsky, Langmuir 9 (1993) 3695.
[14] P.A. Kralchevsky, V.N. Paunov, I.B. Ivanov, K. Nagayama, J. Colloid Interface Sci. 151 (1992) 79.
[15] W.A. Gifford, L.E. Scriven, Chem. Eng. Sci. 26 (1971) 287.
[16] M.A. Fortes, Can. J. Chem. 60 (1982) 2889.
[17] D.Y.C. Chan, J.D. Henry, L.R. White, J. Colloid Interface Sci. 79 (1981) 410.
[18] V.N. Paunov, P.A. Kralchevsky, N.D. Denkov, I.B. Ivanov, K. Nagayama, Colloids Surf. 67 (1992) 138.
[19] P.A. Kralchevsky, V.N. Paunov, N.D. Denkov, I.B. Ivanov, K. Nagayama, J. Colloid Interface Sci. 155 (1993) 420.
[20] V.N. Paunov, P.A. Kralchevsky, N.D. Denkov, K. Nagayama, J. Colloid Interface Sci. 157 (1993) 100.
[21] P.A. Kralchevsky, K. Nagayama, Langmuir 10 (1994) 23.
[22] P.A. Kralchevsky, V.N. Paunov, N.D. Denkov, K. Nagayama, J. Colloid Interface Sci. 167 (1994) 47.
[23] O.D. Velev, N.D. Denkov, P.A. Kralchevsky, V.N. Paunov, K. Nagayama, J. Colloid Interface Sci. 167 (1994) 66.
[24] P.A. Kralchevsky, V.N. Paunov, K. Nagayama, J. Fluid. Mech. 299 (1995) 105.
[25] P.A. Kralchevsky, V.N. Paunov, N.D. Denkov, K. Nagayama, J. Chem. Soc. Faraday Trans. 91 (1995) 3415.
[26] C.D. Dushkin, H. Yoshimura, K. Nagayama, Chem. Phys. Lett. 204 (1993) 455.
[27] G.S. Lazarov, N.D. Denkov, O.D. Velev, P.A. Kralchevsky, K. Nagayama, J. Chem. Soc. Faraday Trans. 90 (1994) 2077.

[28] A.S. Dimitrov, C.D. Dushkin, H. Yoshimura, K. Nagayama, Langmuir 10 (1994) 432.
[29] M. Yamaki, J. Higo, K. Nagayama, Langmuir 11 (1995) 2975.
[30] K. Nagayama, S. Takeda, S. Endo, H. Yoshimura, Jap. J. Appl. Phys. 34 (1995) 3947.
[31] C.A. Johnson, A.M. Lenhoff, J. Colloid Interface Sci. 179 (1996) 587.
[32] M. Sasaki, K. Hane, J. Appl. Phys. 80 (1996) 5427.
[33] N.D. Denkov, H. Yoshimura, K. Nagayama, Phys. Rev. Lett. 76 (1996) 2354.
[34] N.D. Denkov, H. Yoshimura, K. Nagayama, Ultramicroscopy 65 (1996) 147.
[35] E. Kumacheva, L. Li, M.A. Winnik, D.M. Shinozaki, P.C. Cheng, Langmuir 13 (1997) 2483.
[36] F. Burmeister, C. Schäfle, T. Matthes, M. Bohmisch, J. Boneberg, P. Leiderer, Langmuir 13 (1997) 2983.
[37] S. Rakers, L.F. Chi, H. Fuchs, Langmuir 13 (1997) 7121.
[38] S. Matsushita, T. Miwa, A. Fujishima, Langmuir 13 (1997) 2582.
[39] J. Boneberg, F. Burmeister, C. Schafle, P. Leiderer, D. Reim, A. Fery, S. Herminghaus, Langmuir 13 (1997) 7080.
[40] P.C. Ohara, J.R. Heath, W.M. Gelbart, Angew. Chem. Int. Ed. Engl. 36 (1997) 1078.
[41] N. Bowden, A. Terfort, J. Carbeck, G.M. Whitesides, Science 276 (1997) 233.
[42] S.V. Kukhtetskii, L.P. Mikhailenko, Doklady Academii Nauk 357 (1997) 616.
[43] H. Shibata, H. Yin, T Emi, Philos. Trans. Roy. Soc. London A 356 (1998) 957.
[44] F. Burmeister, C. Schäfle, B. Keilhofer, C. Bechinger, J. Boneberg, P. Leiderer, Adv. Mater. 10 (1998) 495.
[45] K.P. Velikov, F. Durst, O.D. Velev, Langmuir 14 (1998) 1148.
[46] H. Aranda-Espinoza, A. Berman, N. Dan, P. Pincus, S. Safran, Biophys. J. 71 (1996) 648.
[47] S.L. Mansfield, D.A. Jaywickrama, J.S. Timmons, C.K. Larive, Biochim. Biophys. Acta 1382 (1998) 257.
[48] T. Gil, J.H. Ipsen, O.G. Mouritsen, M.C. Sabra, M.M. Sperotto, M. Zuckermann, in: B. de Kruijff (Ed.), Lipid-protein interactions, Biochim. Biophys Acta: Biomembranes, Elsevier, Amsterdam, 1998.
[49] C. Allain, M Cloitre, J. Colloid Interface Sci. 157 (1993) 261.
[50] C. Allain, M Cloitre, J. Colloid Interface Sci. 157 (1993) 269.
[51] C.M. Mate, V.J. Novotny, J. Chem. Phys. 94 (1991) 8420.
[52] M.L. Forcada, M.M. Jakas, A. Gras-Marti, J. Chem. Phys. 95 (1991) 706.
[53] A. Marmur, Langmuir 9 (1993) 1922.
[54] G. Debregeas, F. Brochard-Wyart, J. Colloid Interface Sci. 190 (1997) 134.
[55] O.P. Behrend, F. Oulevey, D. Gourdon, E. Dupas, A.J. Kulik, G. Gremaud, N.A. Burnham, Applied Physics A 66 (1998) 219.
[56] H. Suzuki, S. Mashiko, Applied Physics A 66 (1998) 1271.
[57] J. Lucassen, Colloids Surf. 65 (1992) 131.
[58] E. Janke, F. Emde, F. Lösch, Tables of higher functions, McGraw-Hill, New York, 1960.
[59] M. Abramowitz, I.A. Stegun, Handbook of mathematical functions, Dover, New York, 1965.
[60] G.A. Korn, T.M. Korn, Mathematical handbook, McGraw-Hill, New York, 1968.
[61] P.A. Kralchevsky, K.D. Danov, N.D. Denkov, Chemical physics of colloid systems and interfaces, in: K.S. Birdi (Ed.), Handbook of surface and colloid chemistry, CRC press, Boca Raton, 1997.
[62] C. Camoin, J.F. Roussell, R. Faure, R. Blanc, Europhys. Lett. 3 (1987) 449.
[63] H.B. Dwight, Tables of integrals and other mathematical data, Macmillan Co, New York, 1961.
[64] O.D. Velev, N.D. Denkov, V.N. Paunov, P.A. Kralchevsky, K. Nagayama, Langmuir 9 (1993) 3702.
[65] C.D. Dushkin, P.A. Kralchevsky, H. Yoshimura, K. Nagayama, Phys. Rev. Lett. 75 (1995) 3454.
[66] C.D. Dushkin, P.A. Kralchevsky, V.N. Paunov, H. Yoshimura, K. Nagayama, Langmuir 12 (1996) 641.
[67] Rose et al., Phys. Rev. Lett. 23 (1969) 655.
[68] J.T. Petkov, N.D. Denkov, K.D. Danov, O.D. Velev, R. Aust, F. Durst, J. Colloid Interface Sci. 172 (1995) 147.
[69] H. Brenner, L.G. Leal, J. Colloid Interface Sci. 65 (1978) 191.
[70] H. Brenner, L.G. Leal, J. Colloid Interface Sci. 88 (1982) 136.

[71] K.D. Danov, R. Aust, F. Durst, U. Lange, J. Colloid Interface Sci. 175 (1995) 36.
[72] J.T. Petkov, K.D. Danov, N.D. Denkov, R. Aust, F. Durst, Langmuir 12 (1996) 2650.
[73] P.S. Laplace, Traité de mécanique célste; suppléments au Livre X, 1805.
[74] R. Finn, Equilibrium capillary surfaces, Springer-Verlag, New York, 1986.
[75] P.A. Kralchevsky, J.C. Eriksson, S. Ljunggren, Adv. Colloid Interface Sci. 48 (1994) 19.
[76] B.V. Derjaguin, Kolloidn. Zh. 17 (1955) 207.
[77] I.B. Ivanov, P.A. Kralchevsky, in: I.B. Ivanov (Ed.), Thin liquid films, Marcel Dekker, New York, 1988, p. 49.
[78] B.V. Derjaguin, Dokl. Akad. Nauk SSSR 51 (1946) 517.
[79] I.B. Ivanov, P.A. Kralchevsky, A.D. Nikolov, J. Colloid Interface Sci. 112 (1986) 97.
[80] P.A. Kralchevsky, I.B. Ivanov, J. Colloid Interface Sci. 137 (1990) 234.
[81] S.U. Pickering, J. Chem. Soc. 91 (1907) 2001.
[82] Th. F. Tadros, B. Vincent, In: P. Becher (Ed.) 'Encyclopedia of emulsion technology'. New York: Marcel Dekker, 1983;1:129.
[83] N.D. Denkov, I.B. Ivanov, P.A. Kralchevsky, J. Colloid Interface Sci. 150 (1992) 589.
[84] H.M. Princen, The equilibrium shape of interfaces, drops, and bubbles, in: E. Matijevic (Ed.), Surface and colloid science, vol. 2, Wiley, New York, 1969, p. 1.
[85] C. Dietrich, M. Angelova, B. Pouligny, J. Phys. II France 7 (1997) 1651.
[86] B. Pouligny private communication.
[87] D.E. Ingber, Ann. Rev. Physiol. 59 (1997) 575.
[88] D.E. Ingber, Scientific American, January 1998, p. 30.
[89] J.D. Robertson, J. Cell. Biol. 19 (1963) 201.
[90] R. Henderson, P.N.T. Unwin, Nature 257 (1975) 28.
[91] A. Baroin, A. Bienvenue, P.F. Devaux, Biochemistry 18 (1979) 1151.
[92] P.N.T. Unwin, G. Zampighi, Nature 283 (1980) 545.
[93] A.K. Mitra, M.P. McCarthy, R.M. Stroud, J. Cell Biol. 109 (1989) 755.
[94] R. Henderson, J.M. Baldwin, T.A. Ceska, F. Zemlin, E. Beckmann, K.H. Downing, J. Mol. Biol. 213 (1990) 899.
[95] S. Marcelja, Biochim. Biophys. Acta 455 (1976) 1.
[96] H. Schröder, J. Chem. Phys. 67 (1977) 1617.
[97] J.C. Owicki, M.W. Springgate, H.M. McConnell, Proc. Natl. Acad. Sci. USA 75 (1978) 1616.
[98] J.C. Owicki, H.M. McConnell, Proc. Natl. Acad. Sci. USA 76 (1979) 4750.
[99] P. Joost, O.H. Grifith, R.A. Capaldi, G. Vanderkooi, Biochim. Biophys. Acta 311 (1973) 141.
[100] J.H. Davis, D.M. Clare, R.S. Hodges, M. Bloom, Bochemistry 22 (1983) 5298.
[101] M. Esmann, A. Watts, D. Marsh, Biochemistry 24 (1985) 1386.
[102] E. Favre, A. Baroin, A. Bienvenue, P.F. Devaux, Biochemistry 18 (1979) 1156.
[103] G. Benga, R.P. Holmes, Prog. Biophys. Mol. Biol. 43 (1984) 195.
[104] M. Bloom, E. Evans, O.G. Mouritsen, Quart. Rev. Biophys. 24 (1991) 293.
[105] Y.S. Chen, W.L. Hubbel, Exp. Eye Res. 17 (1973) 517.
[106] J. Davoust, A. Bienvenue, P. Fellmann, P.F. Devaux, Biochim. Biophys. Acta 596 (1980) 28.
[107] B.A. Lewis, D.M. Engelman, J. Mol. Biol. 166 (1983) 203.
[108] J.C. Huschilt, R.S. Hodges, J.H. Davis, Biochemistry 24 (1985) 1377.
[109] J. Riegler, H. Möhwald, Biophys. J. 49 (1986) 1111.
[110] J. Peschke, J. Riegler, H. Möhwald, Eur. Biophys. J. 14 (1987) 385.
[111] O.G. Mouritsen, M. Bloom, Biophys. J. 46 (1984) 141.
[112] M.M. Sperotto, O.G. Mouritsen, Eur. Biophys. J. 19 (1991) 157.
[113] N. Dan, P. Pincus, S.A. Safran, Langmuir 9 (1993) 2768.
[114] N. Dan, A. Berman, P. Pincus, S.A. Safran, J. Phys. II France 4 (1994) 1713.
[115] S.J. Bussell, D.L. Koch, D.A. Hammer, J. Fluid. Mech. 243 (1992) 679.
[116] J.G.H. Joosten, in: I.B. Ivano (Ed.), Thin liquid films, Marcel Dekker, New York, 1988, p. 569.